Journal of Structural Geology 32 (2010) 537–553

Contents lists available at ScienceDirect

Journal of Structural Geology

journal homepage: www.elsevier.com/locate/jsg

Small-scale faulting in the Upper Cretaceous of the Groningen block (The Netherlands): 3D seismic interpretation, fault plane analysis and regional paleostress

Heijn van Gent [a,*], Stefan Back [b], Janos L. Urai [a], Peter Kukla [b]

[a] Structural Geology, Tectonics and Geomechanics, RWTH Aachen University, Lochnerstraße 4-20, Haus A, D-52056 Aachen, Germany
[b] Geological Institute, RWTH Aachen University, Wüllnerstraße 2, D-52056 Aachen, Germany

ARTICLE INFO

Article history:
Received 7 July 2009
Received in revised form
24 February 2010
Accepted 9 March 2010
Available online 16 March 2010

Keywords:
Upper Cretaceous chalk
Paleostress
Fault surface undulations
Seismic interpretation
Fault plane analysis

ABSTRACT

Over the last years, field-based studies have shown that fault surfaces can exhibit a considerable self-affine topography. It is reasonable to assume that similar undulations are also present in fault interpretations from 3D reflection seismic data, however both the interpretation uncertainty and geophysical resolution limits hinder their analysis. This study analyses a set of small-scale, non-reactivated faults in the Upper Cretaceous Chalk Group (Upper Ommelanden Formation) of the NW-part of the Groningen Block, the Netherlands, in a high quality Pre Stack Depth Migrated 3D seismic data set. The studied faults are fully contained inside the Chalk Group, in an area located between the major tectonic-bounding faults of the NW Groningen Block. Over 200 faults, with offsets in the order of 30–50 m, were interpreted across an area of ca. 150 km^2, showing a clear preferential orientation for strike, dip and dip-direction. Detailed interpretations and 3D fault plane analyses show undulations on the fault plane. We show that these undulations are not an interpretation or gridding artefact, and interpret these to indicate direction of fault slip. These results were used to calculate a paleostress tensor, using all faults to calculate a single stress tensor for the entire study area by Numerical Dynamic Analysis.

Based on the orientation, position and a thickness analysis, it is interpreted that these faults formed due to the tectonic reactivation of salt structures in the Latest Cretaceous. The calculated paleostress state shows a general NW–SE-extension, with a vertical maximum principle stress, and a stress ratio of about 0.3, indicating that the studied faults are not the result of dewatering. This interpretation agrees both with a nearby salt-tectonic reconstruction, as well as field-based paleostress results from the UK, Belgium and France. A first look at other surveys from the Dutch sector indicates that similar faults are present in other areas, with different orientations. We propose that a dedicated analysis of these faults across on- and offshore Europe would allow extending the stress map of the Late Cretaceous into areas where the Chalk is not outcropping.

© 2010 Elsevier Ltd. All rights reserved.

1. Introduction

This work presents a detailed analysis of a set of small-scale faults interpreted on high-quality 3D seismic data of the Upper Cretaceous Chalk Group of the NW Groningen Block, the Netherlands (Fig. 1a). The interpretation results are compared with existing analyses of faults in the chalk of NW Europe, and used for paleostress analysis. Previous studies on small-scale faults in chalk strata have been controversial concerning the interpretation of the origin of faulting. Hibsch et al. (1995) and Hibsch et al. (2003) interpreted intra-Chalk faults to have formed by compaction. In contrast, Vandycke (2002) argued for tectonic deformation as the main cause of faulting observed in Chalk outcrops. The study presented here will help to distinguish between the two models.

Paleostress analyses provide information on the tectonic evolution of the crust and help to predict the location and possible orientations of fracture and fault systems below the resolution of seismic observation. In hydrocarbon exploration, these fracture systems can have economically viable permeabilities (Koestler and Ehrmann, 1991; Arnott and van Wunnik, 1996; van Konijnenburg et al., 2000; Smith and McGarrity, 2001; Otrtuno-Arzate et al., 2003; Casabianca et al., 2007); thus, the seismic-based paleostress-analysis approach can potentially impact oil and gas exploration and production in carbonate

* Corresponding author. Fax: +49 241 80 92358.
E-mail address: H.vangent@ged.rwth-aachen.de (H. van Gent).

0191-8141/$ – see front matter © 2010 Elsevier Ltd. All rights reserved.
doi:10.1016/j.jsg.2010.03.003

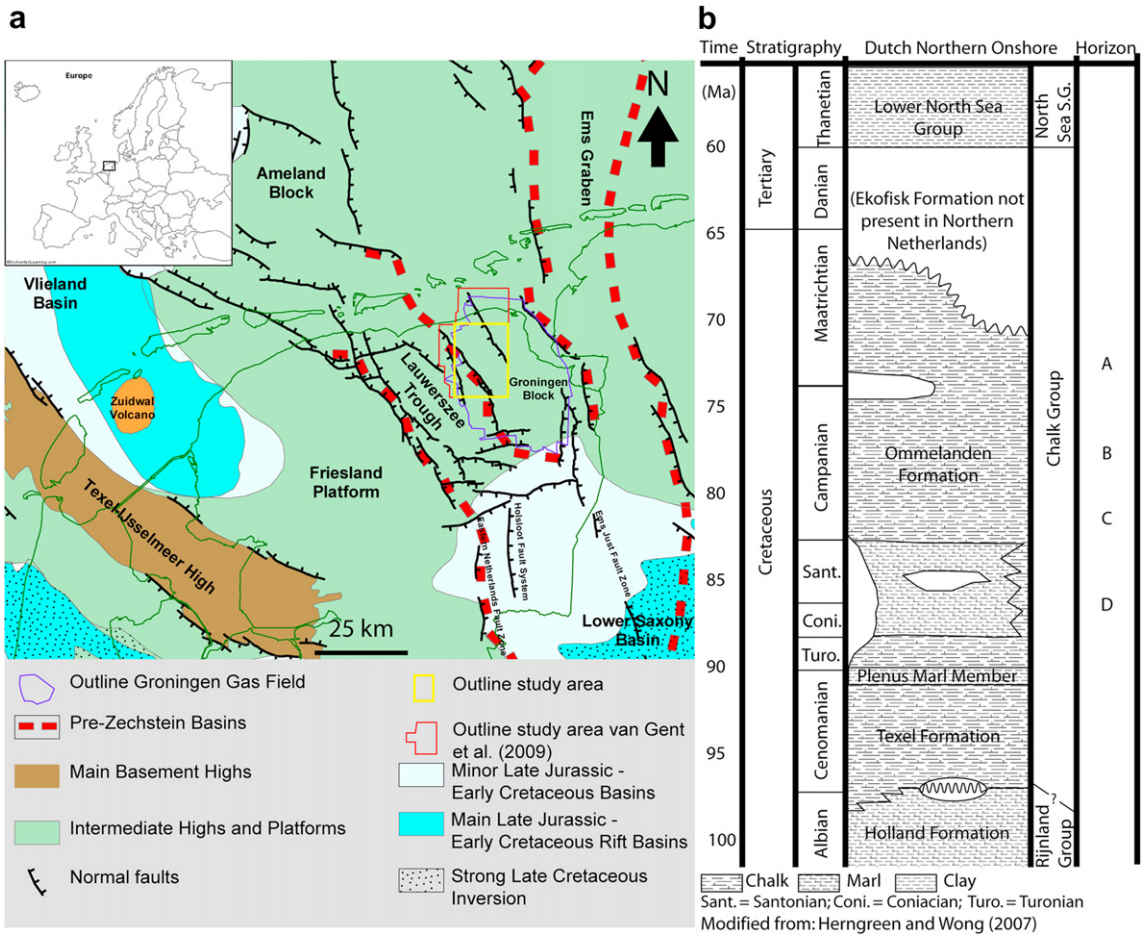

Fig. 1. (a) Location of the study area in the NW of the Groningen High, at the border of the Lauwerszee Trough. Image courtesy of NAM. (b) Simple stratigraphic column for the northern Netherlands. Modified from Herngreen and Wong (2007). Also indicated are the approximate stratigraphic positions of the four internal reflectors (A–D), see Table 1.

provinces in general. Paleostress analyses can be used to estimate the timing of the opening and closing of faults and fractures, and for analyzing and modelling the migration of geofluids (du Rouchet, 1981; Sapra, 1997).

Paleostress analyses are usually based on maps of fault systems at km-scale (e.g. Anderson, 1942; Michon et al., 2003), on the detailed mapping of fault surfaces and slip directions in outcrops at m-scale (Bergerat, 1987; Kleinspehn et al., 1989; Angelier, 1994; Hibsch et al., 1995; Delvaux, 1997; Saintot and Angelier, 2002; Vandycke, 2002; Caiazzo et al., 2006; Sippel et al., 2009), or on the analysis of calcite twins at mm-scale (Turner, 1953; Spang, 1972; Larroque and Laurant, 1988; Rocher et al., 2004). With the increased availability of industrial 3D seismic data for the scientific community, several attempts have been made to extract (paleo-) stress tensors from 3D seismic data (this does not include papers on seismic processing that constrain the orientation of either fractures or the present-day stress tensor, such as Neves et al., 2003). Seismic extraction of paleostress has the advantage that direct access to rocks is no longer required, so that sedimentary cover, or seawater coverage in offshore settings does not hinder paleostress analysis. Furthermore, the fact that seismic data is often available in areas of hydrocarbon exploration or production means that the results are directly applicable to aid the local exploration/production strategy (du Rouchet, 1981; Gartrell and Lisk, 2005; Henk, 2005; Lohr, 2007; Van Gent et al., 2009). For example, Gartrell and Lisk (2005) have used 3D seismic data to calculate the present-day stress field in the Timor Sea (N Australia). Lohr (2007) used 3D seismic data to constrain the stresses that caused deformation of the Top Rotliegend in the Central European Basin. Finally, Van Gent et al. (2009) showed how reactivated faults in reflection seismic data can be used to calculate paleostress stratigraphy in the NW part of the Groningen Block (Fig. 1) by using structural reconstructions, matching of horizon shapes across faults, and the analysis of undulations of fault planes.

In this study, a set of small-scale (on a seismic scale, the faults are actually roughly the same size as structures used in field-based paleostress study) faults (<50 m offset) of the Upper Cretaceous Chalk Group is interpreted and analyzed in detail (Figs. 2 and 3). These faults have low offset, are fully contained inside the Chalk Group, and not reactivated by later tectonic phases. To differentiate these small-scale faults from large, long-living, cross-formational faults, we use the term “Intra-Chalk faults”. This term reflects that the studied faults do not penetrate Top or Base of the Chalk Group; but is not meant to imply syn-sedimentary faulting. Using several overlapping and detailed interpretations of a number of these faults, it will be shown that these faults commonly have a down-dip oriented undulation, which is not the result of imaging or interpretation artefacts. These undulations can be used to constrain the slip direction in the down-dip-direction (pure normal faulting). Assuming that all faults slipped in a similar fashion as the faults studied in detail, we used the orientation and related slip direction of all faults spread over the 10 × 15 km study area to calculate the regional paleostress tensor at the time of development of these faults. This approach differs from “normal” field-based paleostress

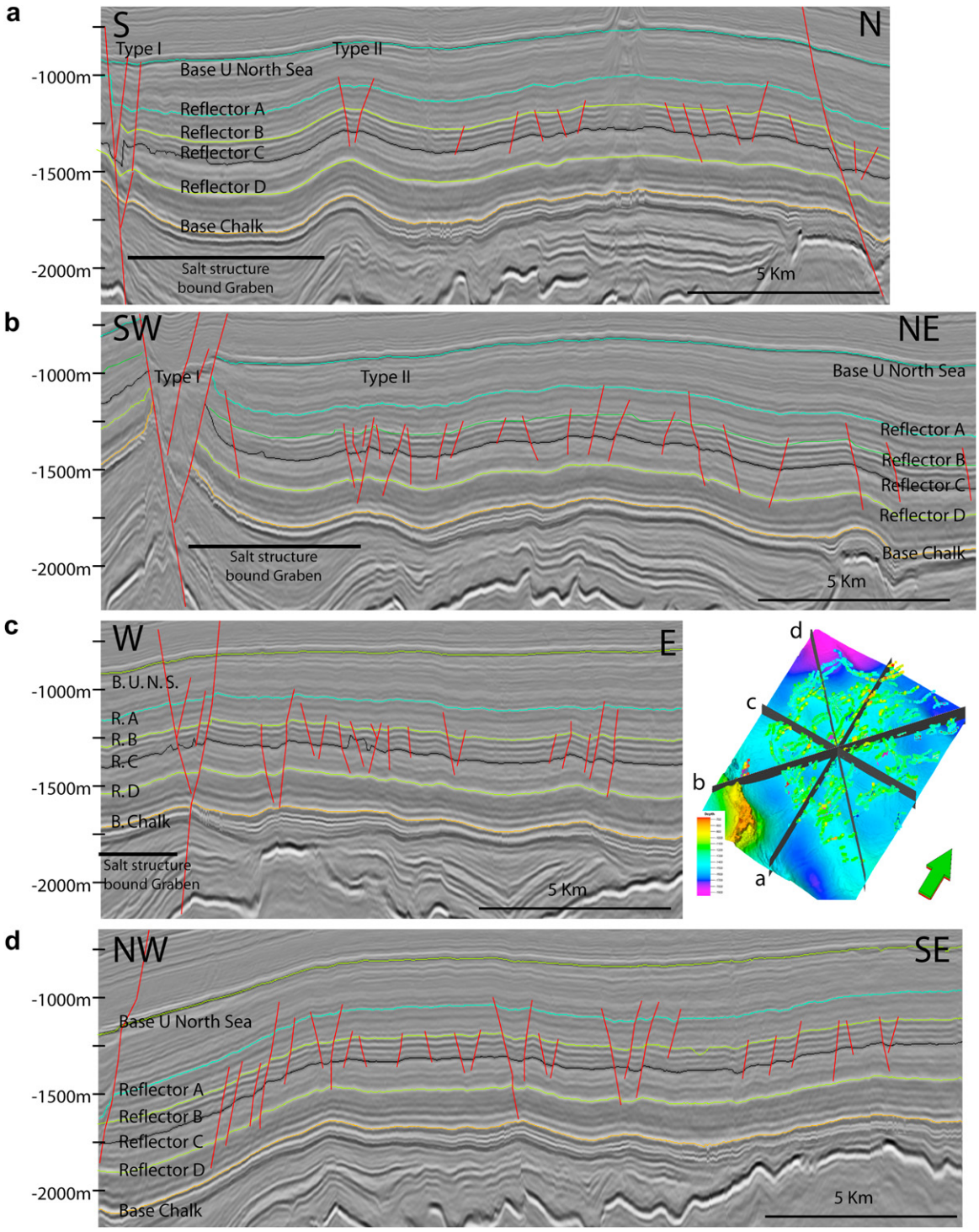

Fig. 2. Four seismic crosssections (a–d) of part of the Groningen high. Although some meso-faults are interpreted, a high number of small-throw faults are observed between Base Upper North Sea and Base Chalk reflectors. Orientations of the crosssections are indicated in the inset. Indicated with "Salt structure bound Graben" is the Graben that is also indicated in Figs. 3f and 5f and discussed in the text.

studies in two important aspects: Firstly, this approach does not use direct fault observations from the field, where usually slickenlines or slickenfibers are used to constrain slip-direction (Means, 1987). Since these are much too small (in the order of 1–5 mm) to be observed in seismic data, a different approach of constraining the slip-direction as is required (also see: Gartrell and Lisk, 2005; Lohr, 2007; Van Gent et al., 2009). The second aspect deals with the size of the study area. In field-based paleostress studies, it is a common approach to compare a number of outcrop-scale (3–300 m) paleostress tensors with each other to gain insight into the regional (10–100 km) differences in stress state. In this work we use all visible faults (faults above seismic resolution) in the study area to calculate a single regional paleostress tensor for this area. It must be noted that we use "regional" in this paper only as

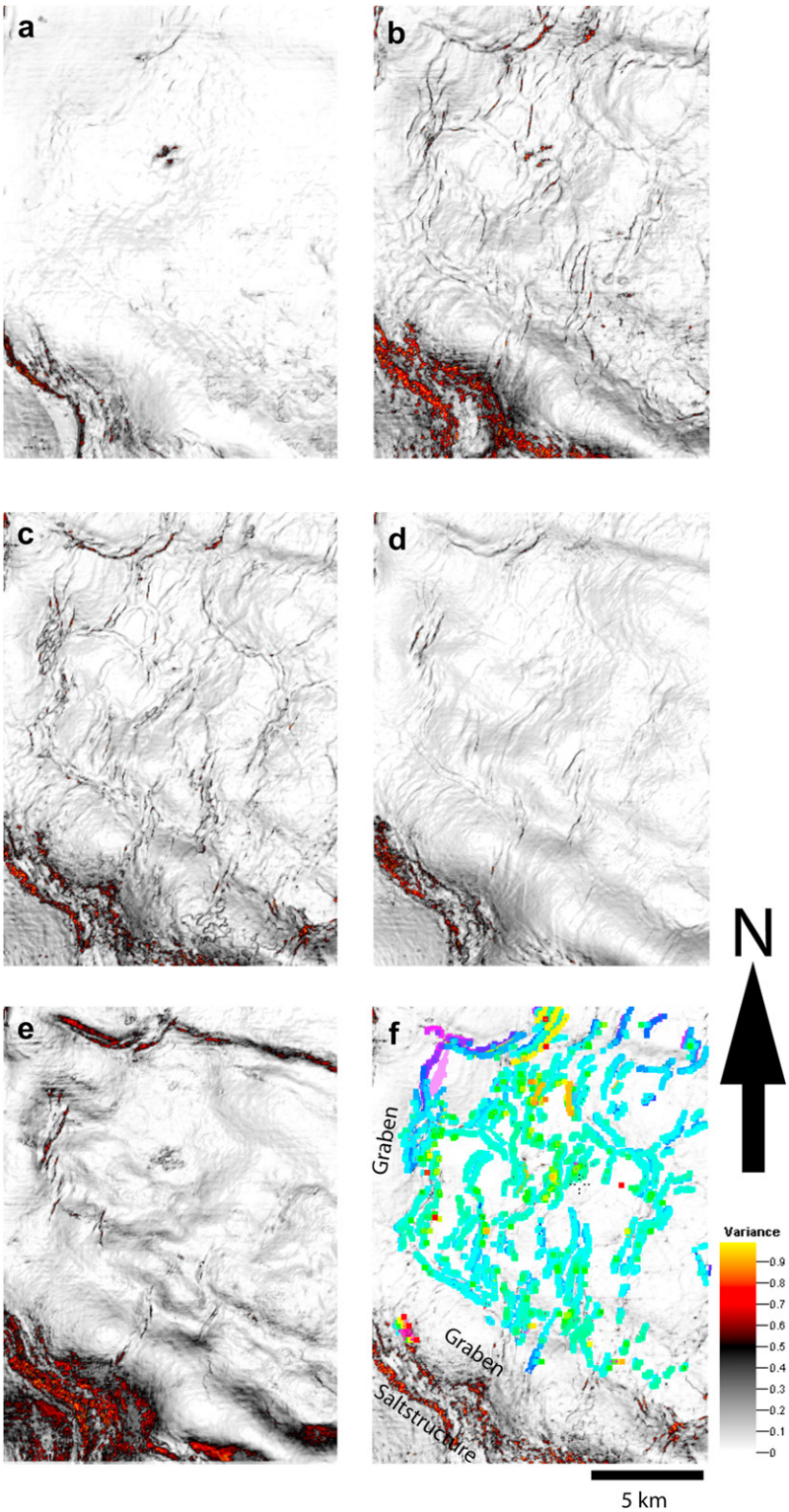

Fig. 3. Variance maps of the five reflectors in Fig. 2. (a) Variance map of the base of the North Sea Super-Group. (b) Variance map of reflector B. (c) Variance map of reflector C. (d) Variance map of reflector D. (e) Variance map of the base of the Chalk Group. (f) Variance map of reflector B with all interpreted fault sticks.

a comparative term, larger than the study area, but the exact size is not determined. The regional character of the stress tensor does not allow the observation of stress permutations on smaller scales (which is possible in comparative field paleostress studies), but gives the larger scale stress state. However, if one were to compare the paleostress results from several seismic blocks, an insight in the basin-wide stress changes, both over time and space, can be gained. The calculated stress tensor agrees well with that obtained also by (Van Gent et al., 2009) for the same area and time from larger, reactivated faults. While the latter was also seismic derived, field studies from France, the UK and Southern Belgium show similar results (Vandycke, 2002).

2. Geological setting

The Groningen Block (Fig. 1a) contains one of the largest gas reservoirs of the world. It is part of the North Netherlands High (TNO-NITG, 2004; Wong et al., 2007), and has been a relatively stable block since the Late Kimmerian inversion phase (Latest Jurassic), when the North Netherlands High formed (Stäuble and Milius, 1970; Kettel, 1983; Duin et al., 2006; Wong et al., 2007). From Late Permian to Late Jurassic times, the Groningen Block was part of the Southern Permian Basin. The Rotliegend (Middle Permian) sandstones form the reservoir in the Groningen area, and are sealed by the Late Permian Zechstein evaporites and carbonates (Glennie, 1998; Wong et al., 2007). Triassic to Lower Cretaceous sequences of the Groningen area are only poorly developed on the Groningen Block (TNO-NITG, 2004; Duin et al., 2006; Wong et al., 2007), most likely reflecting a structurally elevated position of the area during this time. The thickness of the Triassic to Lower Cretaceous deposits is generally below 200 m in the study area, but reaches thicknesses between 400 m and 800 m in the surrounding sub-basins. Although many hydrocarbon reserves in the North Sea's Central Graben Area are in (fractured) Chalk Group reservoirs (Koestler and Ehrmann, 1991; Stewart and Clark, 1999; Mallon and Swarbrick, 2002; Casabianca et al., 2007; Mallon and Swarbrick, 2008), the Upper Cretaceous Chalk in the Netherlands is generally not productive (with the exception of the Harlingen Field; see van den Bosch, 1983). As a result, these deposits are relatively poorly studied (Van der Molen et al., 2005). The Chalk Group of the Dutch subsurface consists of Cenomanian to Danian (lowermost Paleocene), relatively deep marine, mostly bioclastic limestones with local marl interlayers (Herngreen and Wong, 2007). Along the basin fringes more clastic formations are found (e.g.: the Aken and Vaals Formations of Southern Limburg; Herngreen and Wong, 2007). The Dutch Chalk Group deposits generally display highly parallel, continuous, low-amplitude reflectors, characteristic of pelagic, autochthonous chalks (Figs. 2 and 3, Gras and Geluk, 1999; Van der Molen et al., 2005).

In the Groningen Block the Chalk Group lies concordantly on top of the Rijnland Group (Figs. 1b and 2, TNO-NITG, 2004; Herngreen and Wong, 2007). The thickness of the Chalk Group deposits varies between 600 m and 1000 m. Although in the surrounding areas the Laramide inversion (Latest Cretaceous) caused intense uplift, truncation, erosion, faulting and inversion (Ziegler, 1982; Dronkers and Mrozek, 1991; Gras and Geluk, 1999; De Jager, 2003; TNO-NITG, 2004; Worum and Michon, 2005; Wong et al., 2007), the North Netherlands High remained relatively stable with only minor uplift of a local to regional character (Stäuble and Milius, 1970; TNO-NITG, 2004; Van der Molen, 2004; Herngreen and Wong, 2007). Only the uppermost Cretaceous shows signs of erosion of probably less than 100 m (Van der Molen, 2004). Post-Cretaceous sedimentation lead to a burial of the Chalk Group sequences in the study area ranges of 800–1800 m.

In the Netherlands, three formations are recognized in the Chalk Group; the Texel Formation, the Ommelanden Formation and the Ekofisk Formation (Fig. 1b; Van Adrichem-Boogaert and Kouwe, 1993–1997; Oakman and Partington, 1998; Herngreen and Wong, 2007). In the study area and its surroundings, the Lower Chalk Texel Formation is 50–70 m thick. The Ommelanden Formation is up to 1000 m thick, and consists of white, chalky limestones with occasional flint layers (Herngreen and Wong, 2007). While the Turonian part of the formation consists of relatively dense limestones, the Coniacian to Santonian deposits are generally more marl-rich. These are overlain by less marly Campanian and Maastrichtian deposits (Herngreen and Wong, 2007). The hard and dense limestones (informally called Upper Ommelanden deposits) have at their base consolidated calcarenites which grade into massive chalk with flint layers (Van Adrichem-Boogaert and Kouwe, 1993–1997; Herngreen and Wong, 2007). The Ekofisk Formation that forms the Tertiary (Danian) continuation of Cretaceous chalk deposition is not present on the Groningen Block. Studies of non-reservoir Chalk Group deposits (in the Dutch offshore and in the Central North Sea) have shown a high porosity and relatively low permeability (Brasher and Vagle, 1996; Mallon and Swarbrick, 2002; Van der Molen, 2004). The onset of overpressure occurs when the Chalk Group is buried below 1 km, coinciding with a change in compaction mechanism (Van der Molen, 2004). Above the Chalk interval, the clastic Cenozoic North Sea Super-Group consist of predominantly siliciclastic rocks that were deposited from the Thanetian (Early Paleocene) onwards.

2.1. Salt tectonics

Movement of the Late Permian Zechstein evaporite deposits has influenced the younger deposits and tectonics in the Dutch subsurface (Van Adrichem-Boogaert and Kouwe, 1993–1997; TNO-NITG, 2004; Wong et al., 2007). Mohr et al. (2005) showed that salt movement in the nearby Ems Graben was a multiphase process. Three distinct pulses of salt movement, coupled to distinct tectonic phases are recognized. The first phase started almost immediately after salt deposition and lasted to the Middle Keuper (Late Triassic); a second phase occurred from Middle Keuper to Lower Cretaceous. For the Lower Cretaceous no salt movement was recorded, but during the Upper Cretaceous to Lower Tertiary, salt movement was reactivated by compressional tectonics indicated by salt rise and small amounts of horizontal shortening of salt diapirs.

3. Methods

3.1. Seismic data and fault-interpretation workflow

The seismic data used in this study is part of a large, merged, 3D pre-stack depth migrated seismic data set, provided by the Nederlandse Aardolie Maatschappij BV. (NAM, a Shell operated 50–50 joint venture with ExxonMobil). The entire survey covers about 20 × 25 km, but the study area covers roughly 10 × 15 km large seismic cube (see Fig. 1). The horizontal and vertical resolution of the seismic data is 25 m. Well control is provided by about 40 production and exploration wells. We used the interpretation package Petrel 2007 from Schlumberger for our interpretation work.

The Chalk Group of the study area exhibits numerous small-scale faults (see Fig. 2), close to the limit of seismic resolution (Hesthammer and Henden, 2000), that occur predominantly between areas of significant Post-Zechstein faulting (i.e. faults with throws between 50 m and 500 m, usually penetrating from Top Zechstein to middle Tertiary). The intra-Chalk faults can be seen in all crosssection directions (Fig. 2), exhibiting throws between 30 and 50 m.

To constrain possible activity phases of the intra-Chalk faults, four auxiliary reflectors (A–D) were mapped (Figs. 1b and 2), which were subsequently used for a thickness analysis. The ages for reflectors A, B C, and D are constrained by biostratigraphic data (see Table 1 as well as Fig. 1b, van Ojik, personal communication, 2008).

Fault interpretation using amplitude, variance, dip and fault enhancement attributes (e.g. Cox and Seitz, 2007) resulted in the interpretation of 213 individual intra-Chalk faults (Figs. 3f, 4a and b). These faults were interpreted in vertical display with a line spacing of 1–5 (25–125 m), and on depth slices in intervals of 50–200 m. Vertical spacing depended on the size and complexity of the fault. Vertical fault interpretations were preferentially oriented perpendicular to the strike of the faults. As a rule, (i) faults were picked only where the fault was clearly defined in the hanging

Table 1
Ages of the reflectors interpreted on Fig. 2. Stratigraphy is based on Van Adrichem-Boogaert and Kouwe, 1993–1997, ages of reflector A–D are constrained with well data (Van Ojik, personal communication 2008).

Horizon	Group	Age
Base North Sea	Lower North Sea	Tertiary; Thanetian (60 Ma)
Reflector A	Chalk	Early Maastrichtian
Reflector B	Chalk	Campanian
Reflector C	Chalk	Early Campanian
Reflector D	Chalk	Santonian–Coniacian
Base Chalk	Chalk	L. Cretaceous; (E) Cenomanian (97 Ma)

wall of the fault block, and (ii) the fault was preferentially picked where a change in fault dip occurred to avoid picking artefacts. In Fig. 2, a zone in the centre of the Chalk interval is visible where the faults are most clearly imaged (between reflector B and C).

To exclude the possibility that the fault-mapping procedure produced artificial fault undulations, four faults were interpreted at 25 m horizontal line spacing, using several different arbitrary and fully independent interpretation profiles, at an angle to the down-dip-direction (Fig. 4c). In general, a fault interpretation plane can cut the fault at any angle, but ideally a plane perpendicular to the fault (parallel to the down-dip-direction, and perpendicular to the strike) results in the "best" interpretation. By choosing a different "down-dip deviation" (angle between the down-dip-direction and the interpretation plane) for each of these interpretations, we ensured that each interpretation was completely independent. Subsequently, a series of independent surfaces of the same fault were constructed from the interpretations using the Petrel algorithm "Convergent Gridder" (see Petrel 2007 Help), with a grid increment of 10 m and smoothed with a Briggs biharmonic minimum curvature algorithm (Briggs, 1974). The resulting planes of the different fault interpretation directions were then visualized using a look-up table, color-coded according to dip-direction, and finally compared for structural similarity or dissimilarity either verifying fault undulations if persistent, or dismissing undulations as artefacts if incoherent in the different interpretation approaches.

3.2. Paleostress analysis

Following their interpretation, the fault surfaces of the study area were used for a paleostress analysis. The existing methods for paleostress calculation can be subdivided into those that are based on the Wallace and Bott criterion of minimum misfit angles (Wallace, 1951; Bott, 1959; Angelier, 1990), and those based on the Mohr–Coulomb Criterion (Coulomb, 1776; Mohr, 1900), with a high shear-to-normal-stress ratio. All methods require as input the combination of the orientation and slip direction of faults. Here the different methods will only be discussed briefly, for a more extensive and technical discussion the reader is referred Angelier (1990), Ramsay and Lisle (2000) and Sippel et al. (2009).

Wallace (1951) and Bott (1959) showed that the direction of slip on any plane can be predicted, based on the stress tensor and the plane orientation, when slip is assumed to be parallel to the maximum resolved shear stress on the plane. Inverting this principle allows one to calculate the stress tensor, based on fault orientations and observed slip direction. Methods that employ this method are for example the Direct Stress Inversion (DSI) (Angelier, 1979, 1994, 1990) and the Multiple Inversion Method (MIM) (Yamaji, 2000), a modification of DSI for separating inhomogeneous data sets. In Wallace and Bott-based methods, the orientation of the principle stresses and their ratio (R) are varied until a minimum is found in the sum of the squared misfit angles for all faults (i.e. a least square criterion). The misfit angle is the difference between the observed slip direction and the calculated shear stress on the fault. The stress ratio is:

$$R = \frac{(\sigma_2 - \sigma_3)}{(\sigma_1 - \sigma_3)}$$

with σ_{1-3} being the principle stresses of the in-situ stress tensor.

Methods based on the Mohr–Coulomb Criterion (Coulomb, 1776; Mohr, 1900) treat all faults as being newly formed and require a high shear stress – to normal stress – ratio on a fault to form. A further requirement is that the contraction and extension axis lie in the plane defined by the slip direction and the fault plane normal. This makes this method unsuitable for the use with faults with oblique striae (Sperner, 1996). Methods based on the Mohr–Coulomb Criterion include Numeric Dynamic Analysis (NDA; Spang, 1972; Sperner et al., 1993; Sperner, 1996) and the *P–T–B* axes Method (PTB; Turner, 1953; PTB; Sperner et al., 1993). These methods assume an angle of internal friction (Θ, generally assumed as 30° for neo-formed faults, and 45° for reactivated faults, Sperner et al., 1993; Sperner, 1996), neglecting the natural variability of this parameter (Sperner et al., 1993). Both PTB and NDA calculate the orientation of the kinematic axes and the

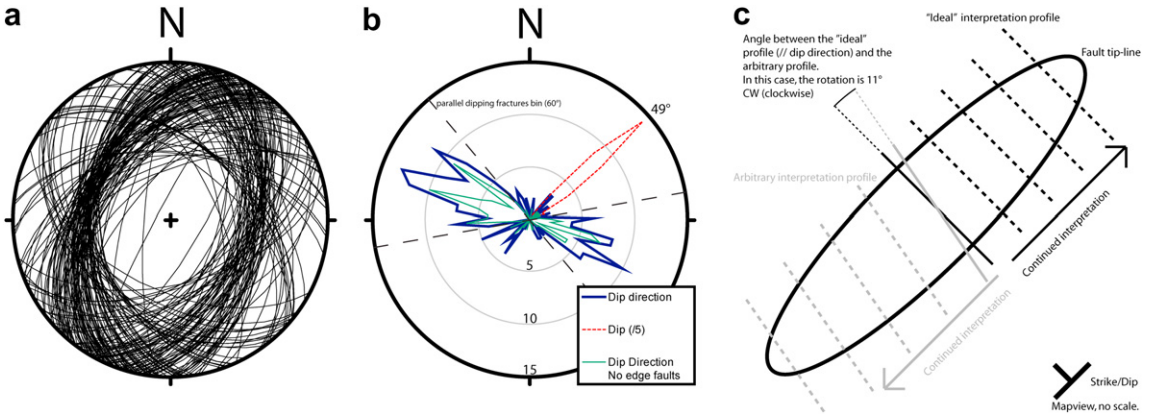

Fig. 4. (a) Stereoplot of the 213 faults interpreted in the Chalk interval. A plot of the Pi-poles are shown in Table 2. (b) Rose diagram, showing the dip-direction (in blue) and the dip angle (in red). The green dip-direction plot shows the orientation of the faults when the faults on the edge of salt structure bound grabens are not taken into account. For dip-direction the concentric gridlines are spaced 5 counts, with a maximum of 15. For dip the concentric gridlines are spaced 25 counts, with a maximum of 75. Orientation bins are 5° wide. (c) Sketch to illustrate the concept of "ideal" interpretation profile and a single arbitray interpretation profile. The ideal profile is parallel to the down-dip-direction, while an arbitrary profile can have any angle to the fault. Since the same fault is sampled with both profiles, the resultant fault plane should have the same geometry (excluding aliasing effects), but since the profiles are slightly different, the different profile represent independent interpretations of the same fault. Here only two profiles are shown, but in Fig. 6 three to four different profiles per fault are shown. The directions of continued interpretation in this figure are arbitrary.

kinematic ratio, but in the case of coaxial, upper crustal deformation these can be considered to coincide with the stress axes and the stress ratio (R) (Anderson, 1942; Huang, 1988; Sperner et al., 1993; Sperner, 1996; Ilic and Neubauer, 2005; Sippel et al., 2009). Several workers combine the Wallace and Bott and Mohr–Coulomb-based methods to calculate solutions that are as realistic as possible (Reches, 1987; Celerier, 1988; Angelier, 1990; Zalohar and Vrabec, 2007; Sippel et al., 2009).

In this study, the paleostress reconstruction program Tectonics FP (Ortner et al., 2002; see also http://www.tectonicsfp.com/) was used, with implementations of several methods. We used the NDA (Spang, 1972; Sperner et al., 1993; Sperner, 1996) and the Right Dihedra Method (Angelier and Melcher, 1977) for our analyses. NDA is preferred for a number of reasons: firstly, DSI fails in cases with a single predominant fault orientation or in conjugate faults, as it requires 4 independent slip directions for the least squared calculation to work properly (Sperner, 1996). The fault set discussed here shows a high degree of conjugation. NDA is specifically suited for neo-formed, conjugate faults, but less for (reactivated) faults with oblique slip (Sperner, 1996). Secondly, earlier tests have shown that NDA is significantly more robust when a modified Monte Carlo analysis was performed (Van Gent et al., 2009; Van Gent, 2010). We believe this results from the least squares algorithm used in DSI, which is very sensitive to outliers and inhomogeneities in the data.

The Right Dihedra Method is a graphic method based on the assumption that when all faults move independently of each other within the same stress, then σ_1 is a part of the P-dihedra of all faults, and σ_3 is a part of all T-dihedra. By overlapping the P–T dihedra, orientation of σ_1 and σ_3 can be constrained, but the solution is not unique and does not include information regarding the relative size of the principal stresses (Angelier, 1979). Unlike NDA however, this method calculates the stress axes, so it was used to confirm the assumption of coinciding kinematic and stress axes.

4. Results

4.1. Thickness analysis and timing of faulting

The study area is surrounded on three sides by a set of sub-basins (see Figs. 2, 3 and 6). The structures are salt-structure bounded grabens, with two types of salt pillows on the flanks (see Fig. 2a and b; note that the crosssections are not ideally oriented for this purpose). On the western side of the graben system, salt pillows with a height of 1800 m are observed (Type I in Fig. 2a and b). The salt does not penetrate the Base Rijnland Group (Lowest Cretaceous). On top of these pillows (Fig. 3), collapse grabens have formed in the Upper Cretaceous and Tertiary deposits. On the eastern side of the graben, less prominent salt pillows (Type II in Fig. 2a and b) formed. As with the larger pillows, Triassic sediments on-lap on the sides and a collapse graben within the Cretaceous sediments are observed. The faults of the collapse graben however do no not extend into the Tertiary. Inside the salt structure bounded grabens between the pillows, tilted Triassic sediments attain a thickness up to 400 m. The symmetrical termination of the Triassic succession against the base of the Lower Cretaceous suggests that the grabens formed before or during the initiation of salt pillow formation. In the study area outside the graben, the Triassic sediments are generally less than 200 m thick. The thickness of the Lower Cretaceous does not change across the salt pillows and graben, and is about 50–90 m.

An analysis of the Zechstein depth map (Fig. 5a) shows that the salt-structure bound grabens are between 400 m and 900 m deeper than the average of the study. Thickness maps show that the grabens were active between Base Upper North Sea and Base North Sea deposition (Fig. 5b), and to a lesser degree between Base North Sea and Base Chalk (Fig. 5c), with the NE–SW striking northern graben section receiving the largest amount of sediment. Between Base Chalk and Base Rijnland (Lowest Cretaceous), no significant differences are observed in the thickness between the graben and other parts of the study area (Fig. 5d), though differences are observed along faults.

4.2. Fault plane analysis

Fig. 3 shows variance horizon maps for reflectors B–D and Top and Base Chalk. The variance maps of Fig. 3 are extracted at the reflector level and faults appear as discrete, narrow zones of high variance (dark). In Fig. 3a, the variance map of the base of the North Sea Group shows only major faults in the SW and NW corners. In the centre of the map, none of the intra-Chalk faults is seen to penetrate the level of the Base North Sea group (compare with Fig. 2). The variance maps of reflectors B and C (Fig. 3b and c) show the predominantly NE–SW trending intra-Chalk faults, although some faults are observed in different orientations. The variance map of reflector D (Fig. 3d) shows mainly NE–SW oriented faults. In the Base Chalk variance map (Fig. 3e), traces of major faults are primarily observed in the N and SW of the survey. As suggested by Fig. 2, the intra-Chalk faults do not penetrate the base of the Chalk Group.

Fig. 4a and b shows that about 80% of the interpreted faults strike NE–SW and ca. 50% of the total numbers of faults (62% of the NE–SW striking faults) dip towards the NW, indicating a parallel-dipping fault array (sensu Buiter et al., 2008). Fault dips range between 45° and 65°, with an average of 49° (Fig. 4b). An oblique view of the interpreted fault sticks is provided in Fig. 5. Fig. 6 shows series of different interpolated fault surfaces for different interpretation directions of four exemplary faults. In the following we use the following definitions: a fault pick is the node where the fault is “picked” during interpretation; a “fault stick” is the 3D representation of all fault picks interpreted in a single interpretation profile, connecting the picks with a bar; the interpretation profile is the 2D (usually vertical) crosssection through a fault on which the fault is picked. The horizontal angle between the down-dip-direction and the interpretation plane in the down dip direction (see Fig. 4c) is given for each fault. CW is a clockwise rotation away from the down-dip-direction; CCW is a counter clockwise rotation. The interpretation direction is also represented by the grey plane in the left of the fault. Fault undulations are defined as consistent, semi-linear changes in dip-directions in the fault plane, with respect to the overall dip-direction. These are interpreted and given as bold lines on the most ideally oriented interpretation of the fault plane (fault interpretation column a). This interpretation is then transposed to the same location on the other fault planes (columns b–d) for comparison. Successful transpositions (undulations that are clearly recognizable and can be independently interpreted on these planes) are black lines, mediocre transpositions (undulations are recognizable, but only with the a-priory interpretation on fault interpretation a) are grey lines. Unsuccessful transpositions (undulations are not recognizable) are grey dashed lines.

The fault plane undulations observed in the first column (Fig. 6a) are recognizable in all of the different interpretations of the four faults shown in Fig. 6. Increasing the deviation of the interpretation profile (away from optimal) shows that the undulations are still recognizable, albeit with slightly different shapes. At higher deviations (>20°), new patterns appear with undulations parallel to the interpretation profile. Overall most undulations have a near down-dip orientation. The fact that in the detail of fault 1a, in the upper right of Fig. 6, multiple fault sticks are present in a single undulation shows that this is not the result of individual fault interpretations slightly out-of-line with the other fault sticks.

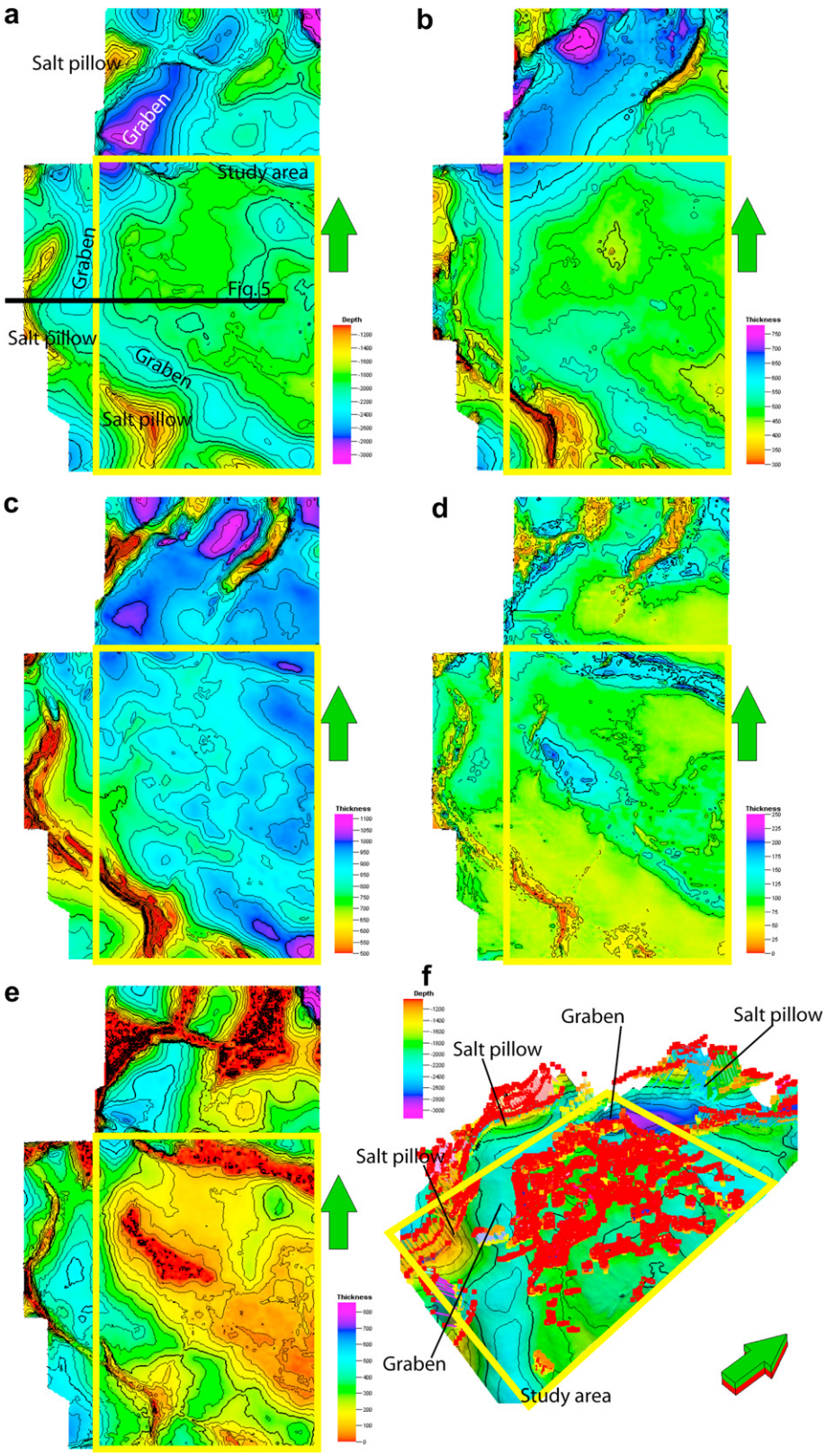

Fig. 5. (a) Top Zechstein depth map with grabens and salt structures indicated. Yellow box indicates present study area from Fig. 3. (b) Thickness between Base Upper North Sea and Base North Sea. (c) Thickness between base North Sea Supergroup and Base Chalk Group. (d) Thickness between Base Chalk and Base Rijnland Formation (Upper Jurassic) (e) Thickness between Base Rijnland and Top Zechstein (f) Oblique view of the Top Zechstein Horizon. Faults within the yellow box are those studied in this study, while the faults along the crests of the salt structures are the meso-faults studied by Van Gent et al. (2009).

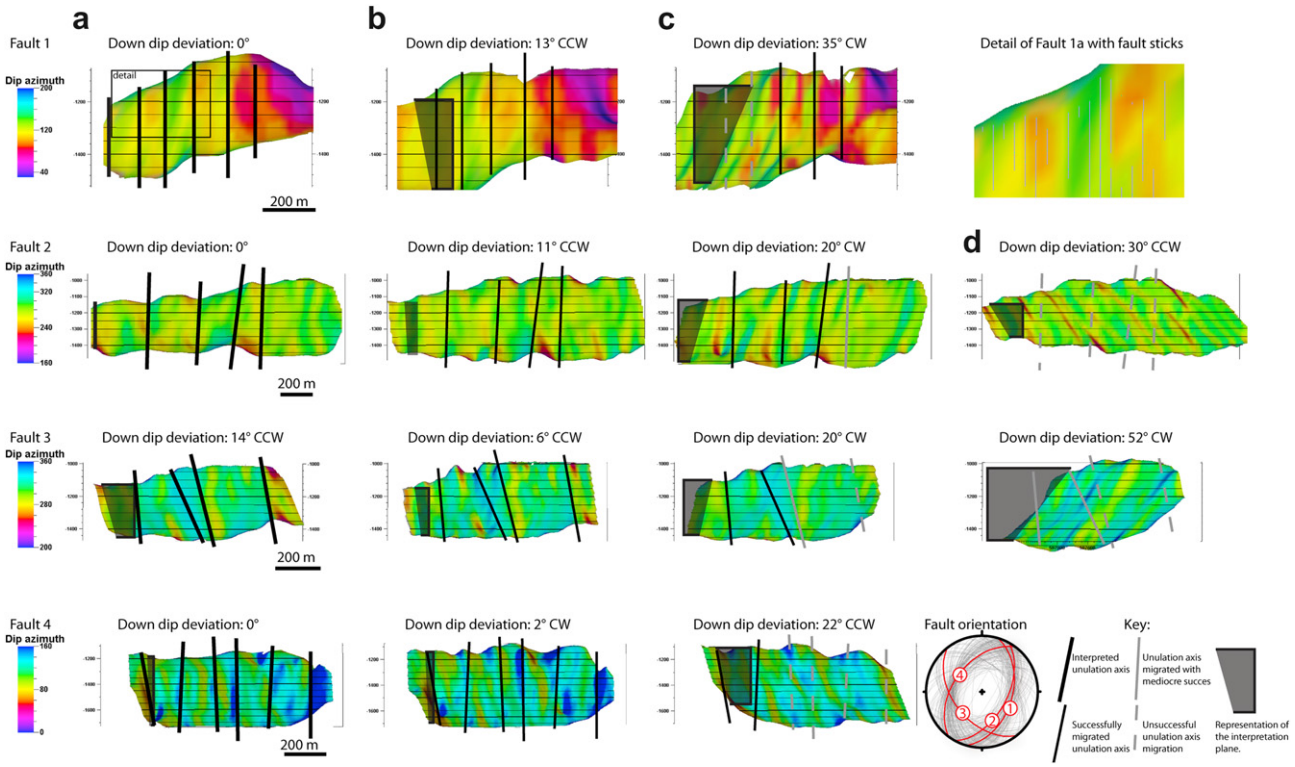

Fig. 6. Overview of the fault surfaces, constructed from the detailed, independent interpretation of four faults from this study area, focussing on the fault undulations, see text for details. Fault 1 is the same fault as described by Van Gent et al. (2009, their Fig. 3), but in a different view. The fault orientations are given in the stereo net. In the upper right a detail of fault 1a is shown, showing the number of fault sticks (purple lines) within an undulation.

To further investigate the robustness of these undulations, Fig. 7a combines all the interpreted picks from all the different interpretations in a single plot. Several horizontal bands of high interpretation density can be distinguished (particularly in fault 4) which are the result of the choice to interpret faults at local dip changes (described above). Despite the presence of these bands, the overall spread of the interpretation points rules out the possibility that the fault surface undulations are an artefact of a longer average vertical distance between the points as compared to the average horizontal distance. Fig. 7b shows the interpolated surface based on the combined data set of all interpreted points (Fig. 7a), with the interpreted undulation axes from (Fig. 6a) shown. This surface shows the main direction of undulations seen in Fig. 6, overprinted together with the undulations forming at high interpretation angles (Fig. 6c and d). The main undulation directions however are still recognizable.

Fig. 8 is an attempt to illustrate the spread of the actual fault picks around the fitted fault surfaces shown in Fig. 6a. The residuals between data and the surface (Fig. 8a) are the spread of interpretation picks around the interpolated fault surface. These are the result of "interpretation noise". The spread of the data is maximum 30 m around the fault plane. Also shown is that (despite the inherent spread in points due to interpretation noise) the vertical bands of high interpretation density (Fig. 8b) show an undulation which has a larger wavelength than the spread in the data. Since the interpreted undulations and the interpolated fault surface are not coaxial (meaning that the undulations do not have linear and parallel axes, see Fig. 8b), it is not possible to find a projection which shows all residuals without parts of the data being obscured by the curved fault. For this reason, in Fig. 8c–g we show 100 m high, (nearly coaxial) ribbons cropped from the data set. Fig. 8c shows fault 4 (see Fig. 6), at 1400 ± 50 m depth (red arrows Fig. 8b), in a projection along the axis of the undulation in this slice. There are clear undulations in the fault pick data, reflected in the shape of the fault plane. Fig. 8d–g shows other fault ribbons viewed in a similar way along the axis of undulations of the fault plane in a suitable slice, but without the fault plane to allow better visual interpretation of the undulations. The horizontal variance of the interpreted points is much smaller than the wavelength of the undulations, which are clearly seen in all figures.

All surfaces in Figs. 6 and 7 are calculated using the default settings of the Taylor Series algorithm (Convergent Gridder in Petrel). To examine if the undulations are dependent on the surface-fitting algorithm, we used (with default settings) six different interpolation methods implemented in Petrel to calculate a fault surface interpretation 'a' of Fault 1 (Fig. 5). Fig. 9 shows the result of this comparison. As expected, some algorithms are less suited to fit a surface covering the whole range of data as they are not meant to interpolate this type of data, but the undulations of Fig. 6a can still be identified in all fault surfaces.

4.3. Interpretation of fault plane analysis results

All faults in Fig. 6 show fault undulation axes from different interpretation profiles can be successfully compared to each other. Whilst nearly all fault undulations are approximately down-dip oriented, Fault 3 seems to exhibit two different undulation orientations that are present in three of the four interpretation directions (Fig. 6, Fault 3, a–c). The reason for this could be that the oblique undulation results from two faults coalescing together (e.g. Lohr et al., 2008). The top tip-line of the fault is lower on the left compared to the right of this undulation, which supports this interpretation. However, it must be noted that the overall

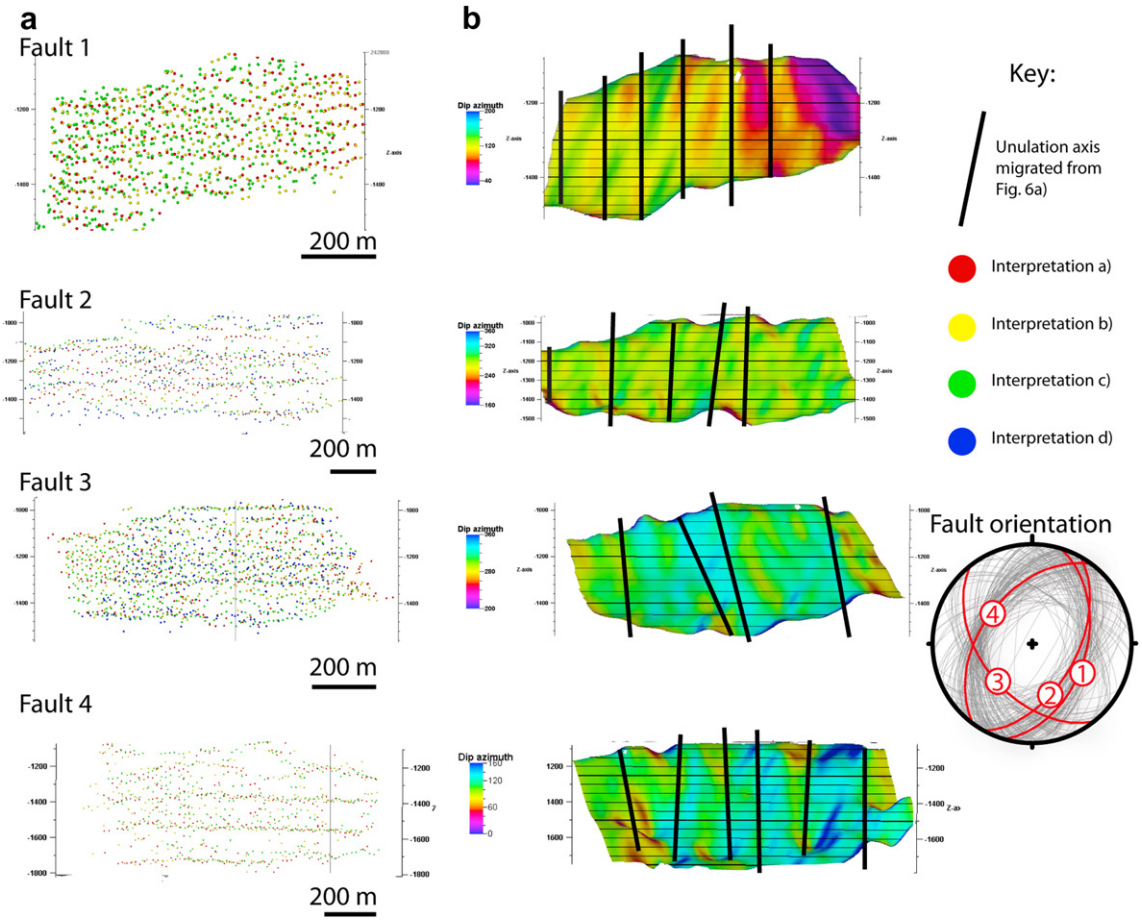

Fig. 7. (a) Original interpretation points for the four different interpretations in Fig. 6. The different colors denote the different interpretations, as in Fig. 6. (b) Fault planes interpolated using the combined interpretations shown in the data from 7(a). The undulation axes shown in the figure are taken from Fig. 6a.

orientation of fault 3 does not correspond to the general trend of the faults in the study area (see stereoplot in Fig. 6). The comparison of fault planes in Fig. 9 shows that the undulations are independent of the gridding algorithm, thus that the undulations in Fig. 6 are not the result of processing artefacts.

A comparison of Figs. 6 and 7 shows consistent undulations of the fault plane. We interpret the observed fault plane undulations to be parallel to the direction of the slip on the fault (e.g. Brown and Scholz, 1985a; Power et al., 1987; Lee and Bruhn, 1996; Renard et al., 2006; Sagy et al., 2007). Slip on the faults studied here is thus interpreted to be dip-slip.

This interpretation is in line with studies of similar fault undulations from different settings and at a very wide range of length scales based on seismic data (see for example Needham et al., 1996; Marchal et al., 2003; Streit and Hillis, 2004; Lohr et al., 2008), laser measurements of exhumed fault surfaces (Renard et al., 2006; Kokkalas et al., 2007; Sagy et al., 2007; Jones et al., 2009; Candela et al., 2009) and other field and laboratory data (e.g. Brown and Scholz, 1985b; Power et al., 1988; Lee and Bruhn, 1996; Van der Zee, 2001). These undulations of the fault plane are usually interpreted to result from the inherent random roughness of a fault at initial failure, which is selectively preserved or even amplified in the direction of the most recent slip (sensu: Brown and Scholz, 1985a; Power et al., 1987; Lee and Bruhn, 1996; Renard et al., 2006; Kokkalas et al., 2007; Sagy et al., 2007). Recent work suggests that faults with large slip are a lot smoother in the slip direction than small-scale faults (Sagy et al., 2007; Lohr et al., 2008).

4.4. Paleostress results

The fault plane analysis indicates that slip on the studied faults is dominantly dip-slip. For the subsequent paleostress analysis, the average orientation of each of the 213 interpreted faults was calculated by fitting an average plane to each fault, then assigning dip-slip movement vectors to each of surface. Table 2 shows the results for this paleostress calculation, together with stereographic projections of the 213 interpreted faults. Since the bulk of the faults is contained between Top and Base Chalk, and do not connect to any other structures, it can be inferred that all faults are neo-formed, non-inherited structures that were not reactivated during the Cenozoic. This supports our choice of the NDA paleostress technique. For NDA-based paleostress estimation, we used an angle of internal friction of 30°, an angle commonly used for neo-formed faults (Sperner et al., 1993; Sperner, 1996). The results from NDA and Right Dihedra give consistent kinematic and stress axes, supporting the robustness of the results. The calculated paleostress axes show a vertical σ_1 and a NNE oriented σ_2. This stress states represents NW–SE extension. The stress ratio for the NDA-calculation has a value of 0.31. The misfit histogram for the NDA-calculation has the half-bell-shape of a homogeneous data set (Sperner et al., 1993; Sperner, 1996).

The analysis described above uses a data set where the most of the shape information of individual faults is lost. In addition, faults are not weighed for their size or the detail of interpretation. To study the effect of this simplification, we have used each triangular segment of the electronic fault planes in combination with the corresponding dip-slip direction to calculate paleostress. This data

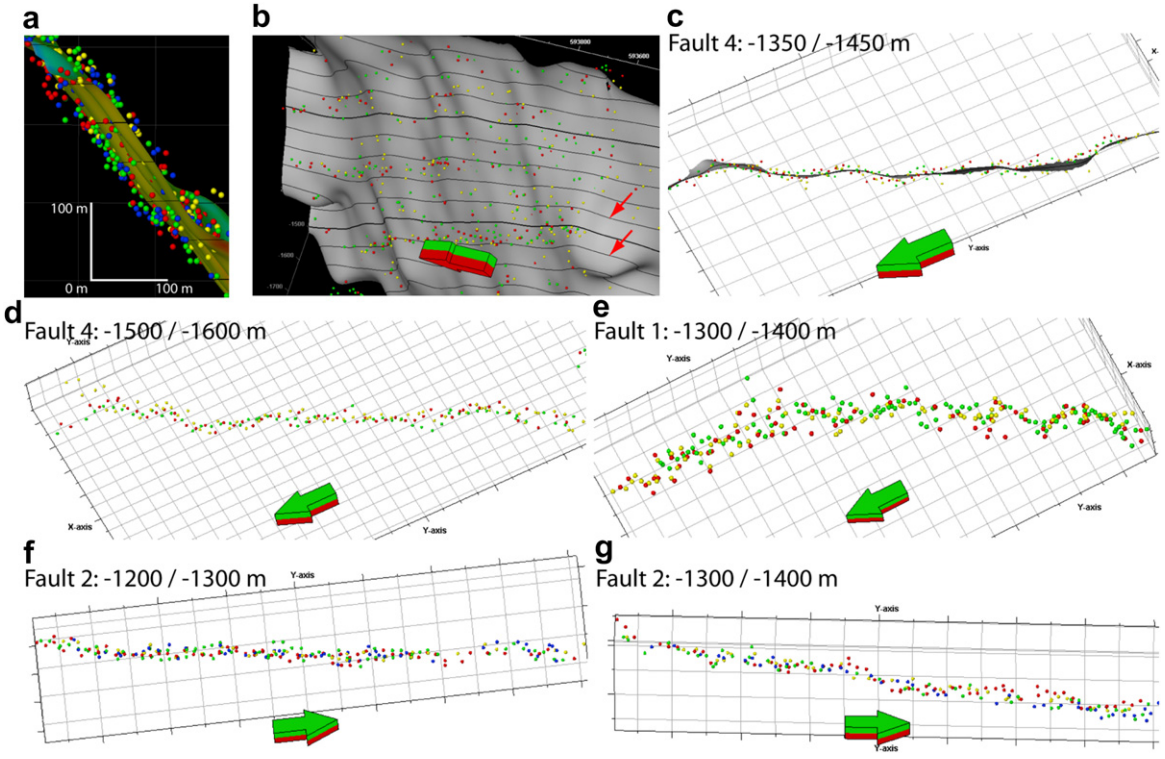

Fig. 8. Detailed observations of the link between fault interpretation and fault surface undulations. For orientation and color key, see Figs. 6 and 7(a) (a) Along-strike view of fault 2, showing the different interpretations as spheres (with color denoting the interpretation in Fig. 6) and the surface Fault 2 a-interpolation (Fig. 6) to indicate the residual distance of the interpretation points relative to the interpolated fault plane. (b) updip, oblique view from the footwall block of fault 4 (For orientation; the arrow points north, green is up, red is down). This image shows the different interpreted points as spheres and fault plane 4a – interpolation (Fig. 6). Note the curving of the interpolated surface at the edges of the fault, deu to interpolation artefacts. (c) Along dip view of a cropped 100 m high ribbon of data from fault 4 around the −1400 m isochore (between red arrows in b). The fault surface is shown for clarity. (d) A 100 m high ribbon of data from fault 4, around the −1550 m isochore. The fault surface is not shown, but was used to orientate the view in an optimal down-dip orientation. (e) as (d) but for fault 1, around the −1350 m isochore. (f) as (d) but for fault 2, around the −1250 m isochore. (g) as (D) but for fault 2, around the −1350 m isochore.

set consists of 7442 orientation/slip pairs. Here we assume that slip is always dip-slip on every part of the fault, but this is an obvious simplification (see for example Roberts, 1996; Morewood and Roberts, 2000; Cowie and Roberts, 2001; Papanikolaou and Roberts, 2007; Maniatis and Hampel, 2008). Table 3 shows the results using this data set. The general shape of the pi-plot density contours is similar in both cases, showing that the simplification of our first analysis is representative for the detailed fault shapes. Both

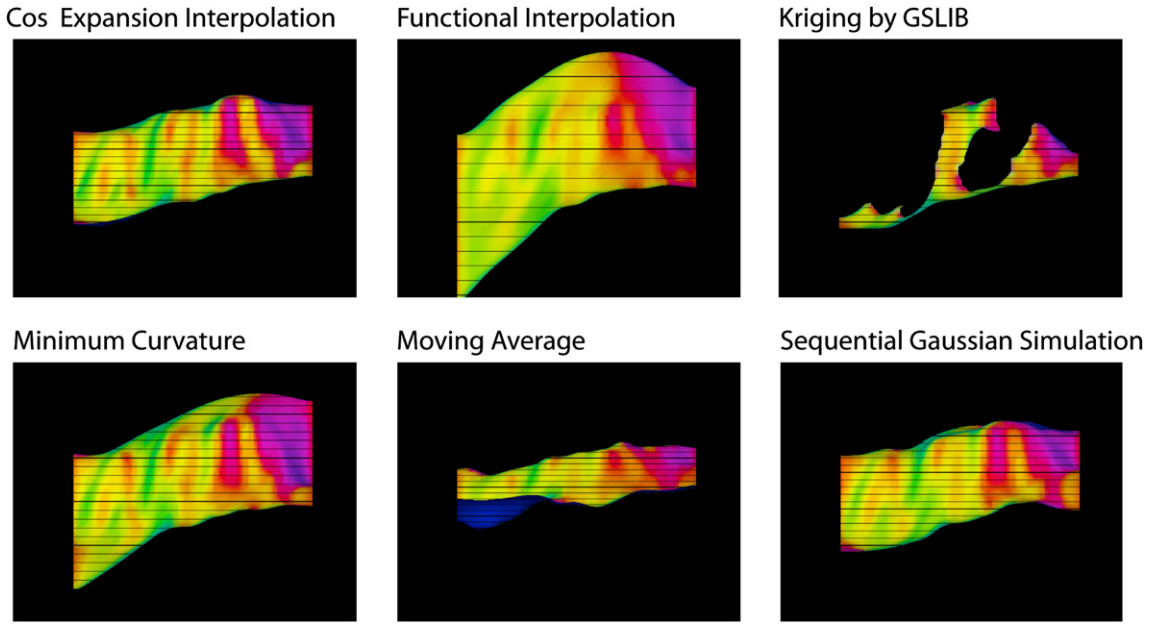

Fig. 9. Comparison of fault planes built using different interpolation methods. The input data is fault 1a (Fig. 6). Fault surface colors denote dip-direction to show undulation as in Figs. 6 and 7. The names of interpolation method are taken from the Petrel 2007 Program. Default calculation settings were used to calculate these fault planes.

Table 2
Paleostress results calculated using a single dip-direction/dip pair for every fault.

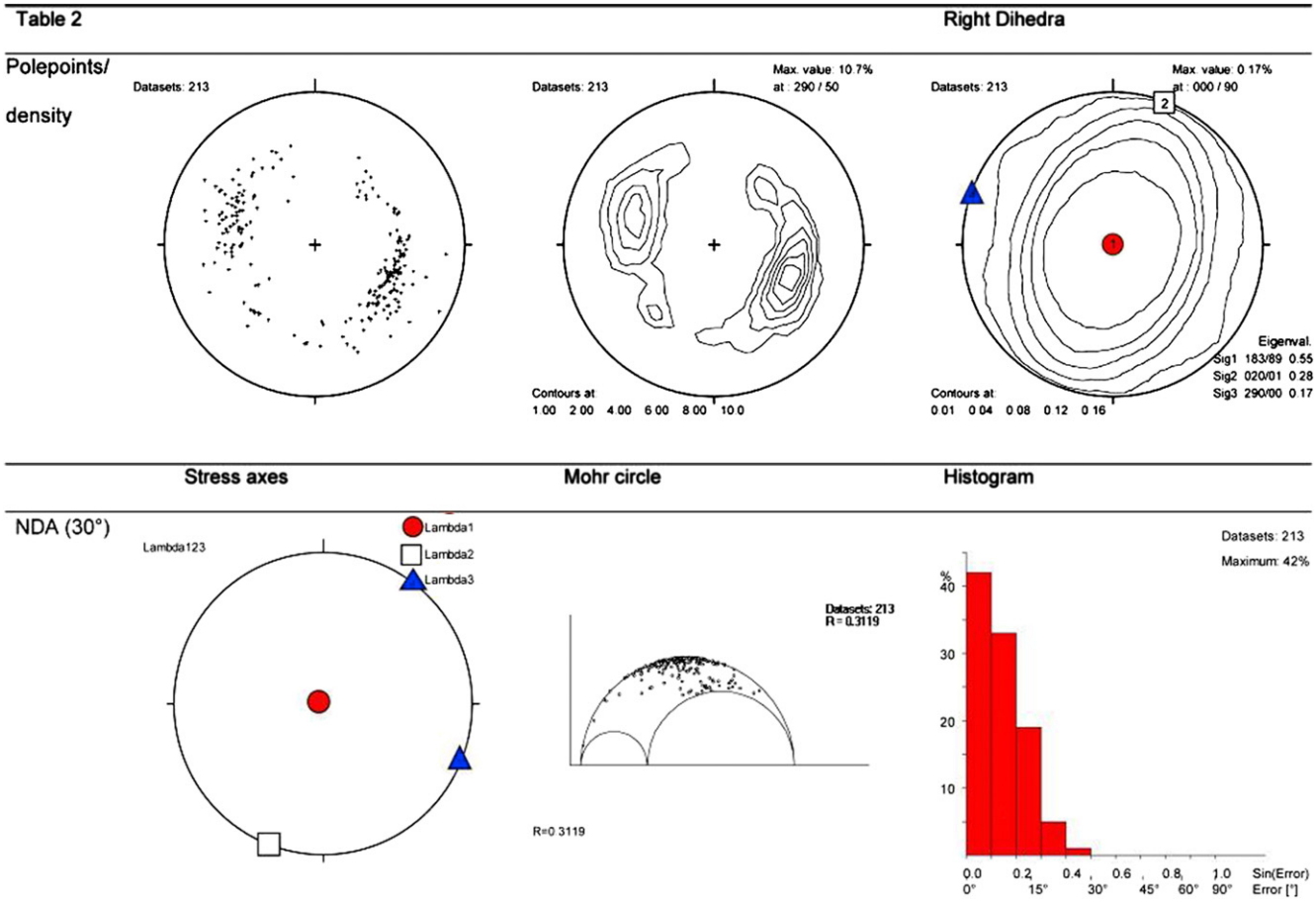

the NDA and the Right Dihedra Method calculated a vertical σ_1 and a NNE oriented σ_2. NDA gave an *R*-value of about 0.27. The NDA and Right Dihedra axes in Table 3 fit well with the axes calculated for Table 2 (the deviation is 1°) and the *R*-value is similar (0.31 vs. 0.27). Also the misfit histograms show a very good result, as 75% of the calculated slip directions have a misfit angle of 10° or less.

5. Discussion

5.1. Fault undulations

We interpret the consistent pattern of dip-direction variations on the fault plane (Figs. 6 and 7) as fault undulations that are not the result interpretation or interpolation artefacts. Fault undulations are observed on a wide range of length scales and are often described to be self affine (Brown and Scholz, 1985a; Power and Tullis, 1991; Lee and Bruhn, 1996; Develi and Babadagli, 1998; Van der Zee, 2001; Sagy et al., 2007; Candela et al., 2009). In this context it has to be kept in mind that "fault surfaces" in outcrops are formed by a combination of fracturing and erosion of a fault zone, and that fault surfaces studied here are representations of an entire zone of deformation with finite thickness and a complex internal structure (compare for example with: Koestler and Ehrmann, 1991; van der Zee et al., 2003). Also the number and particularly the spacing of data points, which are significantly smaller and larger respectively in this seismic study, need to be considered when comparing field and seismic studies.

The fault surface analysis presented in this paper documents that distinguishing "real" undulations from artefacts resulting from differences in the location of the pick in different crosslines, is a challenge. In addition, aliasing can occur if undulations exist at wavelength smaller than twice the sample point distance (Nyquist frequency; Campos and Tututi, 2007; Maxit, 2009). A further complexity occurs when the interpretation plane has a large angle in respect to the down-dip-direction (Fig. 6, Fault 2d and Fault 3d). Here, the interpretation uncertainty in the interpretation direction creates an additional undulation, that overprints the (in this case) down-dip undulation. We suggest that keeping an interpretation profile at angles below 20° in respect to the down-dip-direction will help to avoid this. If discussing seismic-based fault surface analyses, detailed seismic interpretation is sensitive to "interpretation uncertainty", but "conceptional uncertainty" can be another source of error (Bond et al., 2007), which is not entirely excluded here. In this study, no comparative analysis has been made on how "mis-picking" influences our results, but different interpreters are known to provide significantly different horizon interpretations (Rankey and Mitchell, 2003; Bond et al., 2007).

Figs. 6–9 show that the fault plane undulations are consistent in interpretations in different profiles (Fig. 6a–c/d) and have a wavelength greater than the inherent noise of interpretation (Fig. 8). They are also not the result of artefacts in the gridding algorithm (Fig. 9), of heterogeneous sampling or of spatial aliasing (Fig. 7). The amount of smoothing is, based on visual comparison in slices projected parallel to the axis of local undulations (Fig. 8c), a reasonable approximation to separate real undulations from noise.

Table 3
Paleostress results calculated using dip-direction/dip data from every triangle of the interpolated 3D surfaces.

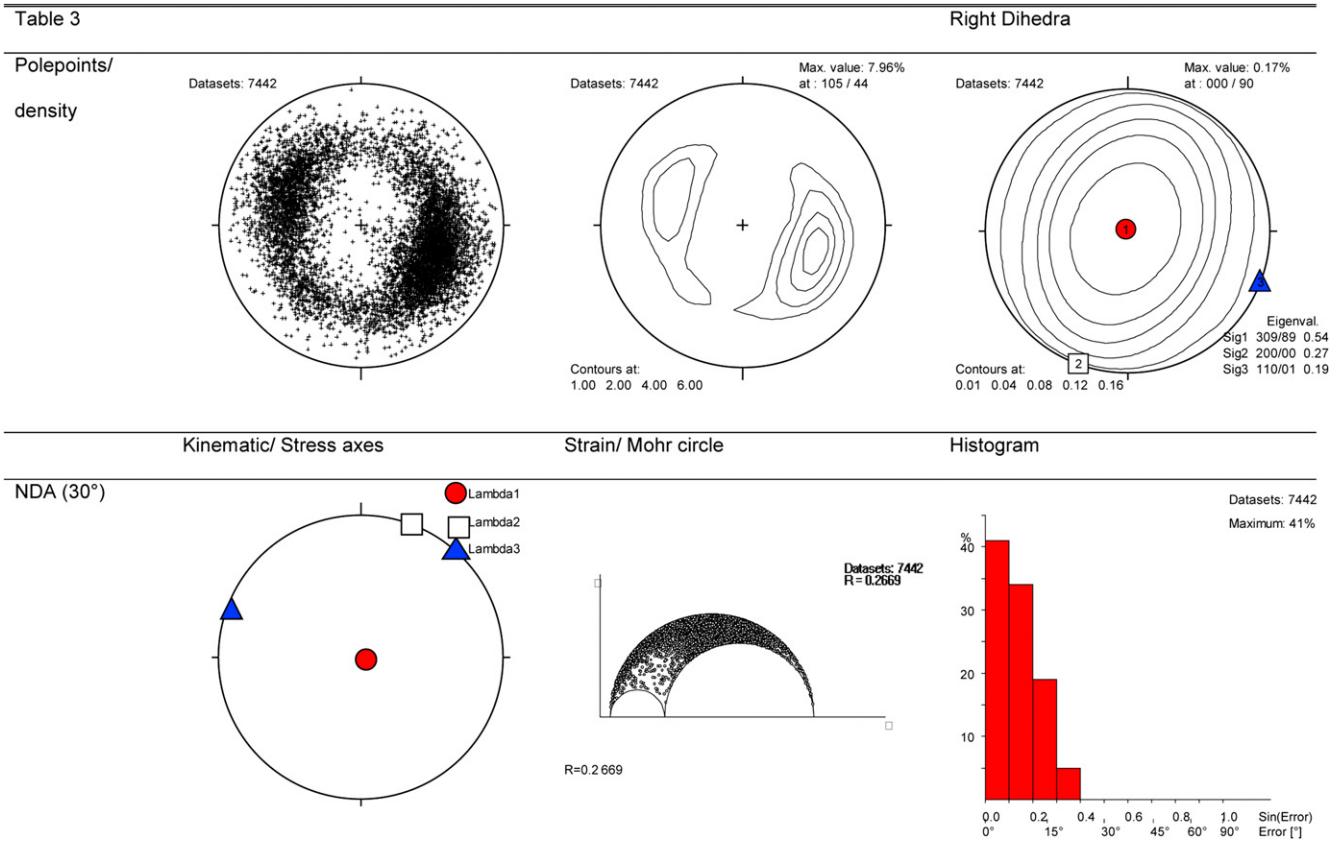

5.2. Geology & regional paleostress

The presence of a large number of faults in the upper Cretaceous Chalk Group of the UK and France was previously interpreted to result of compaction and dewatering (Hibsch et al., 1995; Hibsch et al., 2003). These faults are described to be oriented highly heterogeneously in a single outcrop, contained entirely in the chalk succession, not connected to deeper or shallower structures and to display a pure dip-slip slickenside orientation. Dewatering related Chalk faults are unsuitable for paleostress analysis as their formation is unrelated to tectonic events and due to their highly heterogeneous strike directions. Polygonal faults were first described in the Cenozoic mudrocks of the North Sea and have been identified in over 50 sedimentary basins, predominantly in marine, fine-grained, smectite-rich mudrocks (Cartwright, 1994; Dewhurst et al., 1999; Goulty, 2001; Hansen et al., 2004; Goulty and Swarbrick, 2005). Polygonal faults only rarely occur in chalk (Goulty, 2001; Hansen et al., 2004). One polygonal fault set, reported in the Upper Cretaceous Chalk of the Sable Subbasin, Canadian Atlantic Margin, might have been initiated in underlying mudrocks (Hansen et al., 2004).

On the other hand, Vandycke (2002) argues that the Chalk Group provides an excellent record for brittle tectonics, using observations from several sites in Belgium, France and the UK to extract a paleostress stratigraphy spanning the Upper Cretaceous to the present time. Bevan and Hancock (1986) describe a system of NW-trending fractures in chalk deposits of southern England and northern France, which they attribute to Neotectonic movements in the Lower Rhinegraben system.

The faults of this study have several aspects in common with polygonal faulting. They are restricted to a specific depositional interval, appear to have no preferred strike direction in variance maps (Fig. 4) and low offsets. Detailed analysis of the interpreted faults however shows a clear preferential NW–SW orientation (Fig. 4), and the calculated *R*-value of 0.3 is too high for the radial extension associated with polygonal faulting (the *R*-value for polygonal faulting should approach 0; see Hibsch et al., 2003). Furthermore, a pressure-solutions study in reservoir chalk in the North Sea suggests that the chalk serves as an open system for fluid flow at the (paleo) depth of the Groningen Block (Safaricz and Davison, 2005; Van der Molen et al., 2005). Thus, it is most likely the faults of this study are tectonic in origin.

The analysis of thickness maps (Fig. 5) shows two phases of activity of the major, salt-structure bound grabens; between the middle Upper Cretaceous and the present time, and during the Triassic. Because these grabens are decoupled from the underlying Rotliegend faults by the ductile Zechstein (Roth and Fleckenstein, 2001), and due to the mismatch in orientation of the fault structures across the salt, we infer that the growth of grabens is related to the growth of salt pillows. The thickness analysis then shows that no salt movement occurred in the Groningen Block between the Jurassic and the Campanian corresponding to the conclusion of Mohr et al. (2005). The fact that the salt structures on the western side of the graben extend further into the overburden is interpreted that during the second phase of salt movement, these structures were more active than those on the eastern side. Consequently, it seems most likely that the intra-Chalk faults described in this paper formed as a result of the (re-) activation of flow of salt to the salt pillows on the western side of the graben in the Upper Cretaceous, and the subsequent extension of the cover sediments towards the North West (Mohr et al., 2005).

The faults in this study preferentially dip in the direction of extension, the NW. In a 60° wide bin (stippled lines in Fig. 4b), placed over the average preferred orientation, 105 faults dip in the NW–direction and 64 dip to the SE. Buiter et al. (2008) indicated that parallel, basinward-dipping fault sets in the cover above a moving viscous layer will form when the basal shear on the brittle-viscous transition is "top-to-the-basin-centre". This means that in our case the basal shear was top-to-the NW.

The intra-chalk faults directly bordering the main grabens (Fig. 5) are parallel to these grabens and do not correspond to the overall NW-orientation. A recalculation of the paleostress with 31 of these edge faults removed did not influence the paleostress result, and the interpreted faults still retained the preferential NW–SW strike and NNW dip (Fig. 4b). This suggests that the NW–SE extension was relatively uniform in NW direction, and that the other grabens from Fig. 5 had little influence on this extension. The increase of the thickness of graben fill of the NE–SW striking graben in the NW corner of the study area (Fig. 5) also indicates that Chalk extension was predominantly in the NW direction. Smaller subsidence in the other grabens might have resulted in minor extension in different directions forming faults that do not correspond to the NW–SE extension.

The calculated paleostress results for the small faults in the Groningen area correspond well with the interpretation of the Late Cretaceous stress field derived from the analysis of large-scale faults of the same area (Van Gent et al., 2009). Despite a significant difference of the data sets used, a data set of 27 reactivated faults with a displacement larger than 50 m delivered stress tensors that are almost identical (both in orientation of the principle stresses and stress ratio, which is 0.38; Van Gent et al., 2009) with faults analyzed in this study. Furthermore, Vandycke (2002) observed a very similar pre-Laramide extension phase in the chalks of Kent, Sussex (UK), Boulonnais (France) and the Mons Basin (Belgium). The *R*-value for these tensors is between 0.2 and 0.5 (Vandycke, personal communication, 2008). This suggests that the Late Cretaceous phase of extension is of regional nature.

We have assumed in this study that the slip-direction on the interpreted faults was entirely dip-slip. However, even if the movement on the faults was not exactly dip-slip, but rather normally distributed about pure dip-slip movement, a theoretical Monte Carlo study has shown for three different data sets (Van Gent et al., 2009; Van Gent, 2010) that the introduction of a normally distributed, artificial measurement error in the slip direction, with a standard deviation of several degrees, only has a limited effect on the orientation of the stress axes.

A quick inventory of three additional seismic data sets spread over the entire Dutch sector, suggests that similar intra-Chalk faults are present in seismic surveys as well. All faults in these surveys (in one data set over 230 faults were identified and interpreted) show a preferential E–W orientation, rather than the NE–SW orientation in Groningen. The E–W oriented faults seem generally unaffected by the main tectonic trends of the area. The difference in orientation might result from a difference in timing of fault formation (e.g. Gauthier et al., 2000 observed a Tertiary N–S extension), a perturbation of the local paleostress field (these three additional surveys are west of the Lauwerszee Trough, a Pre-Permian structure, and the present study area is on the eastern side), or a difference in fault-formation mechanism or Zechstein decoupling (e.g. Scheck et al., 2003).

5.3. Mechanical stratigraphy

An important feature of the extensional faults of this study is that they are only visible in the Chalk deposits, and are best observed between auxiliary horizons B and C (Fig. 2). Above and below these horizons the studied faults seem to die out rather quickly. This interval corresponds to the Middle and Upper Campanian. Herngreen and Wong (2007) describe the Campanian and Maastrichtian "Upper" Ommelanden Formation as consisting of consolidated calcarenites in the lower parts that grade towards the top into massive chalks with flint layers. Below the Ommelanden Fm occur marlier Coniacian to Santonian deposits. This makes the Lower to Middle Campanian carbonates relatively competent in comparison with the surrounding Cretaceous chalks and the underlying Triassic rocks, which might explain why these faults predominantly formed in this interval.

5.4. Paleostress assumptions

An important assumption of paleostress analyses is that the sampled stress field is homogenous and constant on the scale of the study. In field studies, outcrop sizes do generally not exceed 50–100 m, though stress deflections are known to occur on this scale (e.g. Dupin et al., 1993; Angelier, 1994; Gruenthal and Stromeyer, 1994; Maerten et al., 2002). Discussions of the validity of the basic paleostress assumptions by e.g. Dupin et al. (1993), Pollard et al. (1993) and Gapais et al. (2000) focus on outcrop scale studies. It is however reasonable to assume that the same features that cause problems in field-based paleostress analyses also influence paleostress analysis at the scale presented.

However, it must be noted that this is probably one of the most important aspects in which this paleostress study differs from field-based paleostress analyses. The area or volume of rock over which the paleostress is calculated is significantly larger than that of field-based paleostress studies. This means that unlike in field studies where local stress states are calculated, a "regional", or possibly, geodynamic stress state is calculated. This also has the effect that a considerable part of internal detail is lost in seismic-based paleostress studies. However, comparing different 3D seismic data sets distributed over a basin will allow recognition of the regional or geodynamical stress changes and their controls. The second aspect in which seismic-based studies differ from field studies is that the slip-direction is not directly observed, but inferred from geometrical information. However, we believe that the fault undulations described here form a reasonable proxy for the paleo-slip direction of faults. On the other hand, the three dimensional nature of seismic data unravels significantly more of the 3D geometry of fault systems than outcrop studies.

To test this first order assumption of stress field homogeneity Van Gent et al. (2009) sub-divided the study area in four zones. Recalculating the stresses with only the faults enclosed in these subareas showed a first order validity of the assumption of stress homogeneity but the result was influenced by the reduction of the amount of faults in the subareas. The present study, with a high number of faults producing the same stress tensor as the large scale study (Van Gent et al., 2009), shows the validity of this approach and indicates that stresses in the Groningen area during the Upper Cretaceous were relatively homogenous on the scale of the analysis. Compared with the Upper Cretaceous stress state calculated in Van Gent et al. (2009), the fact that here only a single set of non-reactivated, low displacement faults is present, makes the structural reconstruction step (in order to remove younger deformation, to obtain older geometries) unnecessary. This makes the results more robust, as the reconstruction is assumed to introduce a lot of errors (Gartrell and Lisk, 2005). This, combined with the observation of similar, but differently oriented intra-Chalk faults in other parts of the Dutch subsurface, leads us to propose that a detailed, NW Europe-wide study of Chalk in seismic

data sets would allow for a detailed stress-map of the Upper Cretaceous in areas currently covered by post-Cretaceous sediments and/or water.

6. Conclusions and outlook

- The workflow described in this paper uses small-scale, intra-Chalk faults, confined to the Cretaceous Chalk Group, to provide a way to estimate paleostress from seismic data for a specific time interval.
- The relatively brittle nature of the Chalk Group makes it an excellent recorder of brittle deformation that might not be observed in softer deposits. The dominance of these faults in a specific interval might be related to variation of brittleness of chalk deposits.
- A detailed interpretation of the fault and the seismic data shows that the fault surfaces studied show clear down-dip undulations that are not the result of interpretation or gridding effects. These undulations are interpreted to represent the paleo-slip direction of these faults.
- The calculated paleostress of this study results in a stress for the Upper Cretaceous that corresponds well with stress fields described by Van Gent et al. (2009) and Vandycke (2002), indicating that the studied faults are very likely to be influenced by a regional stress field.

Acknowledgements

The Nederlandse Aardolie Maatschappij BV (NAM, a Shell operated 50–50 joint venture with ExxonMobil) is thanked both for the use of the seismic data, and for discussion of the results.

Kees van Ojik (Argo Geosciences) is thanked for constraining the age of the chalk reflectors.

We further thank Judith Sippel for various discussions on paleostress and Sussane Buiter for discussing on the nature of parallel dipping fault sets. Schlumberger is thanked for providing Petrel 2007 under academic licence.

Charlotte Krawczyk and an anonymous reviewer are thanked for their comments that improved the manuscript considerably.

References

Anderson, E.M., 1942. The Dynamics Of Faulting And Dyke Formation With Applications To Britain, first ed. Oliver&Boyd, Edinburgh, p. 206.
Angelier, J., 1979. Determination of the mean principle directions of stresses for a given fault population. Tectonophysics 3–4, T17–T27.
Angelier, J., 1990. Inversion of field data in fault tectonics to obtain the regional stress-III. A new rapid direct inversion method by analytical means. Geophysics Journal International 103, 363–376.
Angelier, J., 1994. Fault slip analysis and paleostress reconstruction. In: Hancock, P.L. (Ed.), Continental Deformation. Pergamon Press, Oxford, pp. 53–100.
Angelier, J., Melcher, P., 1977. Sur une methode graphique de recherche des contraintes principales egalement utilisable en tectonique et en seismologie: la methode des diedres droits. Bulletin de la Société Géologique de France 19, 1309–1318.
Arnott, S.K., van Wunnik, J.N.M., 1996. Targeting infill wells in the densely fractured lekhwair field, Oman. GeoArabia 1 (3), 405–416.
Bergerat, F., 1987. Stress fields in the European platform at the time of Africa–Eurasia collision. Tectonics 6 (2), 99–132.
Bevan, T.G., Hancock, P.L., 1986. A late Cenozoic regional mesofracture system in southern England and northern France. Journal of the Geological Society 143, 355–362.
Bond, C.E., Gibbs, A.D., Shipton, Z.K., Jones, S., 2007. What do you think this is? "Conceptual uncertainty" in geoscience interpretation. GSA Today 11, 4–10.
van den Bosch, W.J., 1983. The Harlingen Field, the only gas field in the Upper Cretaceous Chalk of the Netherlands, Petroleum geology of the southeastern North Sea and the adjacent onshore areas. Geologie en Mijnbouw. Netherlands Journal of Geosciences 62, 145–156.
Bott, M.H.P., 1959. The mechanics of oblique slip faulting. Geological Magazine 96 (2), 109–117.
Brasher, J.E., Vagle, K.R., 1996. Influence of lithofacies and diagenesis on Norwegian North Sea chalk reservoirs. AAPG Bulletin 80 (5), 746–769.
Briggs, I.C., 1974. Machine contouring using minimum curvature. Geophysics 39, 39–48.
Brown, S.R., Scholz, C.H., 1985a. Broad bandwidth study of the topography of natural rock surfaces. Journal of Geophysical Research 90 (B14), 12575–12582.
Brown, S.R., Scholz, C.H., 1985b. Closure of random elastic surfaces in contact. Journal of Geophysical Research 90 (B7), 5531–5545.
Buiter, S., Schreurs, G., Ellis, S., 2008. The formation of parallel-dipping faults at passive margins. Geo2008 – resources and risks in the earth system, Aachen, Germany. Schriftreihe der Deutschen Gesellschaft für Geowissenschaften 60, 68.
Caiazzo, C., Ascione, A., Cinque, A., 2006. Late Tertiary–Quaternary tectonics of the Southern Apennines (Italy): new evidences from the Tyrrhenian slope. Tectonophysics 421, 23–51.
Campos, R.G., Tututi, E.S., 2007. Aliasing modes in the lattice Schwinger model. Physics Letters A 36, 1–5.
Candela, T., Renard, F., Bouchon, M., Marsan, D., Schmittbuhl, J., Voisin, C., 2009. Characterization of fault roughness at various scales: implications of three-dimensional high resolution topography measurements. Pure and Applied Geophysics 166 (10–11), 1817–1851.
Cartwright, J.A., 1994. Episodic basin-wide hydrofracturing of overpressured Early Cenozoic mudrock sequences in the North Sea Basin. Marine and Petroleum Geology 11 (5), 587–607.
Casabianca, D., Jolly, R.J.H., Pollard, R., 2007. The machar oil field: waterflooding a fractured chalk reservoir. In: Lonergan, L., Jolly, R.J.H., Rawnsley, K., Sanderson, D.J. (Eds.), Fractured Reservoirs. Geological Society, London, Special Publications, vol. 270, pp. 171–191.
Celerier, B., 1988. How much does slip on a reactivated fault plane constrain the stress tensor? Tectonics 7 (6), 1257–1278.
Coulomb, C.A., 1776. Sur une application des règles maximis et minimis à quelques problèmes de statique à l'architecture. Academie Royale des Sciences: Histoire et Memoires de Mathematique et de Physique 7, 343–382.
Cowie, P.A., Roberts, G.P., 2001. Constraining slip rates and spacings for active normal faults. Journal of Structural Geology vol. 23, 1901–1915.
Cox, T., Seitz, K., 2007. Ant Tracking Seismic Volumes for Automated Fault Interpretation. CSPG CSEG Convention, Calgary, Alberta, Canada.
De Jager, J., 2003. Inverted basins in the Netherlands, similarities and differences. Netherlands Journal of Geosciences/Geologie en Mijnbouw 82 (4), 355–366.
Delvaux, D., 1997. Post-Variscan right-lateral wrench faulting in the Ardenne Allochton and Variscan Front (Belgium). Belgian symposium on structural geology and tectonics. Aardkundige Mededelingen 8, 57–60.
Develi, K., Babadagli, T., 1998. Quantification of natural fracture surfaces using fractal geometry. Mathematical Geology 30 (8), 971.
Dewhurst, D.N., Cartwright, J.A., Lonergan, L., 1999. The development of polygonal fault systems by syneresis of colloidal sediments. Marine and Petroleum Geology 16, 793–810.
Dronkers, A.J., Mrozek, F.J., 1991. Inverted basins of the Netherlands. First Break 9 (9), 409–425.
Duin, E.J.T., Doornenbal, J.C., Rijkers, R.H.B., Verbeek, J.W., Wong, T.E., 2006. Subsurface structure of the Netherlands – results of recent onshore and offshore mapping. Netherlands Journal of Geosciences/Geologie en Mijnbouw 85 (4), 245–276.
Dupin, J.M., Sassi, W., Angelier, J., 1993. Homogeneous stress hypothesis and actual fault slip: a distinct element analysis. Journal of Structural Geology 15, 1033–1043.
Gapais, D., Cobbold, P.R., Bourgeois, O., Rouby, D., de Urreiztieta, M., 2000. Tectonic significance of fault slip data. Journal of Structural Geology 22, 881–888.
Gartrell, A.P., Lisk, M., 2005. Potential new method for paleostress estimation by combining three-dimensional fault restoration and fault slip inversion techniques: first test on the Skua field, Timor Sea. In: Boult, P., Kaldi, J. (Eds.), Evaluating Fault and Cap Rock Seals. AAPG Hedberg Series, 2, pp. 23–26.
Gauthier, B.D.M., Franssen, R.C.W.M., Drei, S., 2000. Fracture networks in Rotliegend gas reservoirs of the Dutch offshore: implications for reservoir behaviour. Geologie en Mijnbouw/Netherlands Journal of Geosciences 79 (1), 45–57.
Glennie, K.W. (Ed.), 1998. Petroleum Geology of the North Sea. Basic Concepts and Recent Advances, fourth ed. Blackwell Science, Oxford, p. 464.
Goulty, N.R., 2001. Polygonal fault networks in fine-grained sediments – an alternative to the syneresis mechanism. First Break 19 (2), 69–73.
Goulty, N.R., Swarbrick, R.E., 2005. Development of polygonal fault systems. A test of hypotheses. Journal of the Geological Society 162, 587–590.
Gras, R., Geluk, M.C., 1999. Late Cretaceous – Early Tertiary sedimentation and tectonic inversion in the southern Netherlands. Geologie en Mijnbouw 78, 1–79.
Gruenthal, G., Stromeyer, D., 1994. The recent crustal stress field in Central Europe sensu lato and its quantitave modelling. Geologie en Mijnbouw 73, 173–180.
Hansen, D.M., Shimeld, J.W., Williamson, M.A., Lykke-Andersena, H., 2004. Development of a major polygonal fault system in Upper Cretaceous chalk and Cenozoic mudrocks of the Sable Subbasin, Canadian Atlantic margin. Marine and Petroleum Geology 21, 1205–1219.
Henk, A., 2005. Pre-drilling prediction of the tectonic stress field with geomechanical models. First Break 23, 53–57.
Herngreen, G.F.W., Wong, T.E., 2007. Cretaceous. In: Wong, T.E. (Ed.), Geology of the Netherlands. Edita-KNAW, Amsterdam, pp. 127–150.
Hesthammer, J., Henden, J.O., 2000. Closing the gasp between theory and practice in seismic interpretation of small-scale faults. Petroleum Geoscience 6, 107–111.

Hibsch, C., Cartwright, J.A., Hansen, D.M., Gaviglio, P., André, G., Cushing, M., Bracq, P., Juignet, P., Benoit, P., Allouc, J., 2003. Normal faulting in chalk: tectonic stresses vs. compaction-related polygonal faulting. In: Van Rensbergen, P., Hillis, R.R., Maltman, A.J., Morley, C.K. (Eds.), Subsurface Sediment Mobilization. Geological Society of London, Special Publications, vol. 216, p. 391.

Hibsch, C., Jarrige, J.-J., Cushing, E.M., Mercier, J., 1995. Paleostress analysis, a contribution to the understanding of basin tectonics and geodynamic evolution. Example of the Permian/Cenozoic tectonics of Great Britain and geodynamic implications in western Europe. Tectonophysics 252, 103–136.

Huang, Q., 1988. Computer-based method to separate heterogeneous sets of fault-slip data into sub-sets. Journal of Structural Geology 10 (3), 297–299.

Ilic, A., Neubauer, F., 2005. Tertiary to recent oblique convergence and wrenching of the Central Dinarides: constraints from a palaeostress study. Tectonophysics 410, 465–484.

Jones, R.R., McCaffrey, K.J.W., Clegg, P., Wilson, R.W., Holliman, N.S., Holdsworth, R. E., Imber, J., Waggott, S., 2009. Integration of regional to outcrop digital data: 3D visualisation of multiscale geological models. 3D GIS and 3D visualisation 35 (1), 4–18.

Kettel, D., 1983. The east Groningen Massif – detection of an intrusive body by means of coalification. In: Kaasschieter, J.P.H., Reijers, T.J.A. (Eds.), Petroleum Geology of the Southeastern North Sea And Adjacent Onshore Areas. Geologie en Mijnbouw 62, The Hague, pp. 203–210.

Kleinspehn, K.L., Pershing, J., Teyssier, C., 1989. Paleostress stratigraphy: a new technique for analyzing tectonic control on sedimentary-basin subsidence. Geology 17, 253–256.

Koestler, A.G., Ehrmann, W.U., 1991. Description of brittle extensional features in chalk on the crest of a salt ridge (NW Germany). In: Roberts, A.M., Yielding, G. (Eds.), The Geometry of Normal Faults. Geological Society Special Publication, vol. 56, pp. 113–123.

Kokkalas, S., Jones, R.R., McCaffrey, K.J.W., Clegg, P., 2007. Quantitative fault analysis at Arkitsa, Central Greece, using terrestrial laser-scanning ("LiDAR". Bulletin of the Geological Society of Greece XXXVII). In: Proceedings of the 11th International Congress, Athens, May 2007, pp. 1–14.

van Konijnenburg, J.-H., Massaferro, J.L., Mauduit, T., Richard, P., Willemse, M., Droste, H., Fenton, M., 2000. Explaining early water breakthrough in a tough carbonate reservoir: the Natih E formation, Al Ghubar Field, Oman. In: AAPG Annual Meeting, New Orleans, Louisiana, April 16–19, 2000.

Larroque, J.M., Laurant, P., 1988. Evolution of the stress field pattern in the south of the Rhine Graben from the Eocene to the present. Tectonophysics 148, 41–58.

Lee, J.-J., Bruhn, R.L., 1996. Structural anisotropy of normal faults. Journal of Structural Geology 18 (8), 1043–1059.

Lohr, T., 2007. Seismic and Sub-seismic Deformation on Different Scales in the NW German Basin. PhD thesis, Freie Universität Berlin.

Lohr, T., Krawczyk, C.M., Oncken, O., Tanner, D.C., 2008. Evolution of a fault surface from 3D attribute analysis and displacement measurements. Journal of Structural Geology 30 (6), 690–700.

Maerten, L., Gillespie, P., Pollard, D.D., 2002. Effects of local stress perturbation on secondary fault development. Journal of Structural Geology 24, 145–153.

Maniatis, G., Hampel, A., 2008. Along-strike variations of the slip direction on normal faults: insights from three-dimensional finite-element models. Journal of Structural Geology 30 (1), 21.

Mallon, A.J., Swarbrick, R.E., 2002. A compaction trend for non-reservoir North Sea Chalk. Marine and Petroleum Geology 19, 527–539.

Mallon, A.J., Swarbrick, R.E., 2008. Diagenetic characteristics of low permeability, non-reservoir chalks from the Central North Sea. Marine and Petroleum Geology 25, 1097–1108.

Marchal, D., Guiraud, M., Rives, T., 2003. Geometric and morphologic evolution of normal fault planes and traces from 2D and 4D data. Journal of Structural Geology 25, 135–158.

Maxit, L., 2009. Wavenumber space and physical space responses of a periodically ribbed plate to a point drive: a discrete approach. Applied Acoustics 70, 563–578.

Means, W.D., 1987. A newly recognized type of slickenside striation. Journal of Structural Geology 9 (5–6), 585.

Michon, L., van Balen, R.T., Merle, O., Pangnier, H., 2003. The Cenozoic evolution of the roer valley rift system integrated at a European scale. Tectonophysics 367, 101–126.

Mohr, M., Kukla, P.A., Urai, J.L., Bresser, G., 2005. Multiphase salt tectonic evolution in NW Germany: seismic interpretation and retro-deformation. International Journal of Earth Sciences (Geologische Rundschau) 94, 914–940.

Mohr, O., 1900. Welche Umstände bedingen die Elastitätsgrenze und den Bruch eines Materials? Zeitschrift de Vereins Deutscher Ingenieure 44 (1524–1530), 1572–1577.

Morewood, N.C., Roberts, G.P., 2000. The geometry, kinematics and rates of deformation within an en échelon normal fault segment boundary, central Italy. Journal of Structural Geology 22, 1027–1047.

Needham, D.T., Yielding, G., Freeman, B., 1996. Analysis of fault geometry and displacement patterns. In: Buchanan, P.G., Nieuwland, D.A. (Eds.), Modern Developments in Structural Interpretation, Validation and Modelling. Geological Society Special Publication, vol. 99, pp. 189–199.

Neves, F.A., Al-Marzoug, A., Kim, J.J., Nebrija, A.L., 2003. Fracture characterization of deep tight gas sands using azimuthal velocity and AVO seismic data in Saudi Arabia. The Leading Edge, 469–475.

Oakman, C.D., Partington, M.A., 1998. Chapter 9: cretaceous. In: Glennie, K.W. (Ed.), Petroleum Geology of the North Sea. Basic Concepts and Recent Advances, fourth ed. Blackwell Science, Oxford, pp. 294–349.

Ortner, H., Reiter, F., Acs, P., 2002. Easy handling of tectonic data: the programs TectonicVB for Mac and Tectonics FP for Windows(tm). see also. Computers & Geosciences 28, 1193–1200. http://www.tectonicsfp.com/.

Otrtuno-Arzate, S., Ferket, H., Cacas, M.-C., Swennen, R., Roure, F., 2003. Late cretaceous Carbonate Reservoirs in the Cordoba Platform and Veracruz Basin, Eastern Mexico. In: Bartolini, C., Buffler, R.T., Blickwede, J. (Eds.), The Circum-Gulf of Mexico and the Caribean: Hydrocarbon Habitats, Basin Formation, And Plate Tectonics. AAPG Memoir 79, 476–514.

Papanikolaou, I.D., Roberts, G.P., 2007. Geometry, kinematics and deformation rates along the active normal fault system in the southern Apennines: implications for fault growth. Journal of Structural Geology 29 (1), 166.

Pollard, D.d., Saltzer, S.D., Rubin, A.M., 1993. Stress inversion methods: are they based on faulty assumptions? Journal of Structural Geology 15 (8), 1045–1054.

Power, W.L., Tullis, T.E., 1991. Euclidean and fractal models for the description of rock surface roughness. Journal of Geophysical Research 96 (B1), 415–424.

Power, W.L., Tullis, T.E., Weeks, J.D., 1988. Roughness and wear during brittle faulting. Journal of Geophysical Research 93 (B12), 15268–15278.

Power, W.L., Tullis, T.E., Brown, S.R., Boitnott, G.N., Scholz, C.H., 1987. Roughness of natural fault surfaces. Geophysical Research Letters 14 (1), 29–32.

Ramsay, J.G., Lisle, R.J., 2000. The Techniques of Modern Structural Geology Volume 3: Applications of Continuum Mechanics in Structural Geology. Academic Press, London, pp. 700–1061.

Rankey, E.C., Mitchell, J.C., 2003. That's why it's called interpretation: impact of horizon uncertainty on seismic attribute analysis. The Leading Edge 22 (9), 820.

Reches, Z.E., 1987. Determination of the tectonic stress tensor from slip along faults that obey the Coulomb yield condition. Tectonics 6 (6), 849–861.

Renard, F., Voisin, C., Marsan, D., Schmittbuhl, J., 2006. High resolution 3D laser scanner measurements of a strike-slip fault quantify its morphological anisotropy at all scales. Geophysical Research Letters 33, L04305.

Roberts, G.P., 1996. Variation in fault-slip directions along active and segmented normal fault. Journal of Structural Geology 18 (6), 835–845.

Rocher, M., Cushing, M., Lemeille, F., Lozac'h, Y., Angelier, J., 2004. Intraplate paleostresses reconstructed with calcite twinning and faulting: improved method and application to the eastern Paris Basin (Lorraine, France). Tectonophysics 387, 1–21.

Roth, F., Fleckenstein, P., 2001. Stress orientations found in north-east Germany differ from the West European trend. Terra Nova 13 (4), 289–296.

du Rouchet, J., 1981. Stress fields, a key to oil migration. AAPG Bulletin 65 (1), 74–85.

Safaricz, M., Davison, I., 2005. Pressure solution in chalk. AAPG Bulletin 89 (3), 383–401.

Sagy, A., Brodsky, E.E., Axen, G.J., 2007. Evolution of fault surface roughness with slip. Geology 35 (3), 283–286.

Saintot, A., Angelier, J., 2002. Tectonic paleostress fields and structural evolution of the NW-Caucasus fold-and-thrust belt from Late Cretaceous to Quaternary. Tectonophysics 357, 1–31.

Sapra, A., 1997. Geological analysis of early water production in horizontal wells in the Middle East. In: AAPG International Conference and Exhibition., Vienna, Austria, Sept. 7–10, 1997, AAPG Bulletin, American Association of Petroleum Geologists: Tulsa, OK, United States, vol. 81, p. 410.

Scheck, M., Bayer, U., Lewerenz, B., 2003. Salt redistribution during extension and inversion inferred from 3D backstripping. Tectonophysics 373, 55–73.

Sippel, J., Scheck-Wenderoth, M., Reicherter, K., Mazur, S., 2009. Paleostress states at the south-western margin of the Central European basin system – application of fault-slip analysis to unravel a polyphase deformation pattern. Tectonophysics – Progress in Understanding Sedimentary Basins 470 (1–2), 129–146.

Smith, R.L., McGarrity, J.P., 2001. Cracking the fractures—seismic anisotropy in an offshore reservoir. The Leading Edge 20, 18–26.

Spang, J.H., 1972. Numerical method for dynamic analysis of calcite twin lamellae. Geological Society of America Bulletin 83 (1), 467–472.

Sperner, B., 1996. Computer programs for the kinematic analysis of brittle deformation structures. In: Frisch, W. (Ed.), Tübinger Geowissenschaftliche Arbeiten Reihe A, 27, Tübingen.

Sperner, B., Ratschbacher, L., Ott, R., 1993. Fault-striae analysis: a Turbo pascal program for graphical presentation and reduced stress tensor calculation. Computers & Geosciences 19 (9), 1361–1388.

Stäuble, A.J., Milius, G., 1970. Geology of Groningen gas field, Netherlands. In: Halbouty, M.T. (Ed.), Geology of Giant Petroleum Fields. American Association of Petroleum Geologists, Tulsa, pp. 359–369.

Stewart, S.A., Clark, J.A., 1999. Impact of salt on the structure of the Central North Sea hydrocarbon fairways. In: Fleet, A.J., Boldy, S.A.R. (Eds.), Petroleum Geology of Northwest Europe: Proceedings of the 5th Conference. Geological Society 65, London, pp. 179–200.

Streit, J.E., Hillis, R.R., 2004. Estimating fault stability and sustainable fluid pressures for underground storage of CO_2 in porous rock. Energy 29, 1145–1456.

TNO-NITG, 2004. Geological Atlas of the Subsurface of the Netherlands – Onshore. TNO-NITG, Utrecht, p. 103.

Turner, F.J., 1953. Nature and dynamic interpretation of deformation lamellae in calcite of three marbles. American Journal of Science 251, 276–298.

Van Adrichem-Boogaert, H.A., Kouwe, W.F.P., 1993–1997. Stratigraphic Nomenclature of the Netherlands; Revision and Update by RGD and NOGEPA, vol. 50. TNO-NITG, Mededelingen Rijks Geologische Dienst, Haarlem. 50.

Van der Molen, A.S., 2004. Sedimentary Development, Seismic Stratigraphy and Burial Compaction of the Chalk Group in the Netherlands North Sea Area. PhD. thesis, Utrecht University.

Van der Molen, A.S., Dudok, H.W., Wong, T.E., 2005. The influence of tectonic regime on chalk deposition: examples of the sedimentary development and 3D-seismic stratigraphy of the Chalk Group in the Netherlands offshore area. Basin Research 17, 63–81.

Van der Zee, W., 2001. Dynamics of fault gouge development in Layers sand-clay sequences. Shaker Verlag, Aachen, PhD thesis.

van Gent, H.W., Back, S., Urai, J.L., Kukla, P.A., Reicherter, K., 2009. Paleostresses of the Groningen area, the Netherlands – results of a seismic based structural reconstruction. Tectonophysics – Progress in Understanding Sedimentary Basins 470 (1–2), 147–161.

Van Gent H.W., 2010. Stress and Strain From 3D Reflection Reflection Data. PhD-thesis RWTH Aachen University, Aachen, Germany.

Vandycke, S., 2002. Paleostress records in Cretaceous formations in NW Europe: extensional and strike-slip events in relationships with Cretaceous-Tertiary inversion tectonics. Tectonophysics 357, 119–136.

Wallace, R.E., 1951. Geometry of shearing stress and relation to faulting. Journal of Geology 59, 111–130.

Wong, T.E., Batjes, D.A.J., de Jager, J. (Eds.), 2007. Geology of the Netherlands. Edita-KNAW, Amsterdam, p. 354.

Worum, G., Michon, L., 2005. Implications of continuous structural inversion in the West Netherlands Basin for understanding controls on Palaeogene deformation. Journal of the Geological Society vol. 162, 73–85.

Yamaji, A., 2000. The multiple inverse method: a new technique to separate stresses from heterogeneous fault-slip data. Journal of Structural Geology 22, 441–452.

Zalohar, J., Vrabec, M., 2007. Paleostress analysis of heterogenous fault-slip data: the gauss method. Journal of Structural Geology 29 (11), 1798–1810.

van der Zee, W., Urai, J.L., Richard, P.D., 2003. Lateral clay injection into normal faults. GeoArabia 8 (3), 501–522.

Ziegler, P.A., 1982. Geological Atlas of Western and Central Europe. Elsevier Scientific Publishing Company, The Hague, Amsterdam, p. 130.